

THESIS

DRAFT TUBE SURGING HYDRAULIC MODEL STUDY

Submitted by

Tony Lee Wahl

Department of Civil Engineering

In partial fulfillment of the requirements

for the Degree of Master of Science

Colorado State University

Fort Collins, Colorado

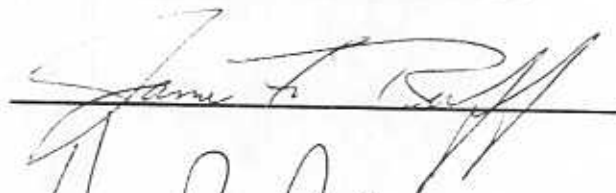
Summer, 1990

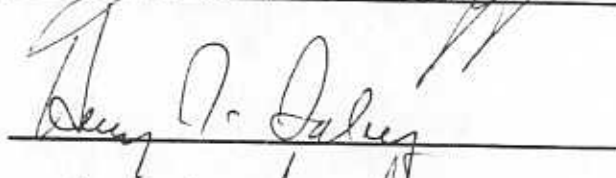
COLORADO STATE UNIVERSITY

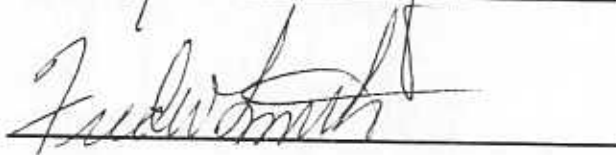
May 10, 1990

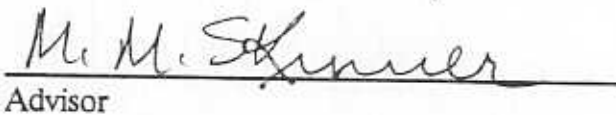
WE HEREBY RECOMMEND THAT THE THESIS PREPARED UNDER
OUR SUPERVISION BY TONY LEE WAHL ENTITLED DRAFT TUBE
SURGING HYDRAULIC MODEL STUDY BE ACCEPTED AS FULFILLING
IN PART REQUIREMENTS FOR THE DEGREE OF MASTER OF SCIENCE.

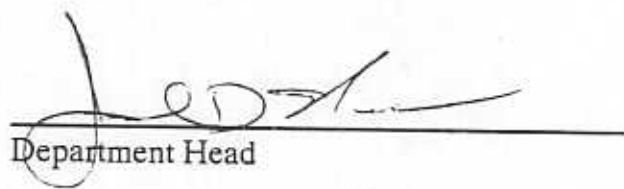
Committee on Graduate Work








Advisor


Department Head

ABSTRACT OF THESIS

DRAFT TUBE SURGING HYDRAULIC MODEL STUDY

The phenomenon of draft tube surging has been investigated using a model hydraulic turbine. Pressure fluctuations at the throat of the draft tube were measured using piezoresistive pressure transducers, and the signals were analyzed using a dynamic signal analyzer and a digitizing oscilloscope. Dimensionless pressure and frequency parameters were calculated for the dominant pressure pulsation at each test point. The dimensionless parameters have been related to the dimensionless swirl parameter of the flow in the draft tube, and maps have been constructed showing the variation of these parameters on the turbine hill curve. In some operating regions the pressure and frequency parameters do not correlate well with the swirl parameter; the pressure and frequency parameter maps constructed on the same axes as the hill curve are preferred for presentation of the test results in these regions.

A twin vortex surging mode has been identified in the model, and the region of its occurrence has been defined on the turbine hill curve. The twin vortex produces pressure pulsations at more than twice the frequency typically associated with draft tube surging. In addition, the relationship of the pressure parameter to the draft tube swirl parameter appears to be affected by the twin vortex. Evidence from the literature suggests that this surging mode also occurs in other nearly homologous units.

A qualitative investigation of the occurrence of synchronous and asynchronous pressure pulsations has been performed. Evidence of synchronous pulsations was obtained at several test points. Recommendations are given for more detailed research in this area.

Tony Lee Wahl
Department of Civil Engineering
Colorado State University
Fort Collins, Colorado 80523
Summer 1990

ACKNOWLEDGMENTS

The successful completion of this research project is due in no small part to the assistance of many people not credited on the title page of this work. Notably, I would like to thank the following for their assistance and support.

My advisor, Dr. Morris M. Skinner, provided an excellent environment for this enjoyable and challenging experience, and also served admirably as laboratory assistant and equipment manager. Along with Dr. Skinner, the members of my Graduate Committee, Dr. Henry T. Falvey, Dr. James F. Ruff, and Dr. Frederick W. Smith, directed and edited this thesis, and provided many helpful suggestions in the planning of this project.

Two organizations deserve special recognition. The Colorado State University Civil Engineering Department funded this research, and the U.S. Bureau of Reclamation donated the test facility to Colorado State. Several Reclamation employees provided valuable assistance. Mr. Brent Mefford aided with calibration of the wicket gates and shake-down tests of the model turbine. His suggestions in the early stages of this project are greatly appreciated. Mr. Tom Isbester was a source of inspiration and excellent advice on the finer points of turbine model operation. His little black book and attention to detail were invaluable in ensuring the safe installation and operation of the turbine test stand. Mr. Phil Burgi and Mr. Cliff Pugh helped to arrange the transfer of the test stand to Colorado State University. Mr. Bob Brennan, Mr. Kerry Sheaman, Mr. Gale Murphy, and Mr. Jerry Davis, each of the Colorado State University Engineering Research Center Shop, were instrumental in the installation of the model at Colorado State.

The friendship and advice of Fred Ogden during the preparation of this thesis is greatly appreciated. Scott Townsend aided with maintenance of the turbine model and provided valuable stress relief as a hunting and fishing companion of the highest caliber.

Finally, the support of my family throughout my educational career has been invaluable. I can never fully repay their efforts.

TABLE OF CONTENTS

CHAPTER 1: Introduction	1
CHAPTER 2: Literature Review	8
2.1 General Overview and Classifications of Surging	8
2.1.1 Asynchronous Surging	9
2.1.2 Synchronous Surging	10
2.2 Field Experiences	11
2.3 Remedial Measures	12
2.3.1 Air Admission	12
2.3.2 Structural Modifications	13
2.4 Vortex Breakdown	14
2.4.1 Vortex Structure	15
2.4.2 Hydraulic Jump Analogy	15
2.5 Model-Prototype Similarity	16
2.5.1 Air Model Tests	16
2.5.2 Hydraulic Model Tests	18
CHAPTER 3: Theoretical Considerations	20
3.1 Dimensional Analysis	20
3.2 Calculation of the Swirl Parameter	21
3.2.1 Wicket Gate Momentum Parameter	22
3.2.1.1 Graphical Analysis	23
3.2.1.2 Potential Flow Analysis	24
3.2.2 Swirl Extracted by the Runner	26
3.3 Application to Prototype Installations	27
CHAPTER 4: Experimental Equipment and Procedures	29
4.1 Test Facility	29
4.2 Experimental Procedure	30
4.3 Wicket Gate Setting	31
4.4 Pressure Fluctuation Measurements	32
4.4.1 Frequency Spectra	32
4.4.2 Phase Relationships	34
4.5 Problems	34
CHAPTER 5: Analysis and Results	35
5.1 Reduction of the Data Set	35
5.2 General Observations	37
5.2.1 Onset of Surging	37
5.2.2 Vortex Breakdown	41
5.2.3 Twin Vortex	42
5.2.4 Higher Frequency Surge	46
5.3 Frequency Parameter	46
5.4 Pressure Parameter	49
5.5 Harmonics	49
5.6 Synchronous and Asynchronous Surging	53

CHAPTER 6: Conclusions and Recommendations	56
6.1 Conclusions	56
6.2 Recommendations for Further Research	58
REFERENCES.....	61
APPENDIX A: Pressure Fluctuation Data	65
APPENDIX B: Model-Prototype Sample Calculation	71
APPENDIX C: Calibrations	75

LIST OF TABLES

Effect of tailwater levels on pressure fluctuations	36
Surge inception data	40
Dominant pressure fluctuation data	66
All model test data	67
Wicket gate calibration	77

LIST OF FIGURES

Hydraulic turbine components	2
Helical vortex in draft tube surging region	4
Vortex breakdown in the flow over a highly swept delta wing	5
Turbine efficiency hill curve	7
Wicket gate definition sketch	23
Wicket gate momentum parameter	25
Schematic of pressure transducer locations	33
Efficiency hill curve and draft tube surging test points	38
Draft tube swirl parameter map	39
Swirl parameter at surge inception	40
Phase of pressure fluctuations in single vortex region	42
Photograph of twin vortex	43
Phase of pressure fluctuations in twin vortex region	44
Comparison of single and twin vortex frequency spectra	45
Frequency parameter map	47
Frequency parameter vs. draft tube swirl parameter	48
Pressure parameter map	50
Pressure parameter vs. swirl for all gate settings	51
Pressure parameter vs. swirl by gate setting	51
Effect of non-sinusoidal pressure fluctuations	52
Differences in pressure pulsation amplitude	54
Test points with evidence of synchronous surging	55
Pressure transducer calibrations	76

CHAPTER 1

INTRODUCTION

In recent years hydroelectric power plants have assumed a specialized role in the scheme of electric power production. Hydroelectric units are increasingly being used to provide peaking power, while large thermal and nuclear plants are used primarily to meet base load. The base load plants operate at maximum efficiency, with a minimum of transient operation, while the peaking units follow the transient portion of the power demand curve. Hydroelectric units are well suited to this task, as quick startup, shutdown, and adjustment of power output are required. However, as a result of this role, hydropower units must also operate reliably over a wide range of operating conditions. One of the greatest obstacles to be overcome in meeting this requirement is the problem of draft tube surging.

Figure 1-1 shows the typical elements of a hydraulic turbine. The draft tube is designed to convey the flow from the exit of the turbine runner to the tailrace, with a minimum of energy loss. Draft tube surging is an unsteady flow occurring in the draft tube as the result of excessive swirl in the flow leaving the turbine runner at off-design operating points. The draft tube surge is characterized by the presence of a helical vortex in the flow, the motion of which produces undesirable, periodic pressure pulsations (pressure surges) within the draft tube. These pressure pulsations produce exciting forces that can affect components of the hydraulic, structural, mechanical, and electrical systems of a power plant. The flow associated with draft tube surging is classified as unsteady because the flow field within the draft tube varies with time; the discharge from the draft tube may or may not vary with

time. The phenomenon is restricted to reaction type turbines, and is generally associated with units having fixed blade runners, either Francis type or axial flow (Dériaz, 1960).

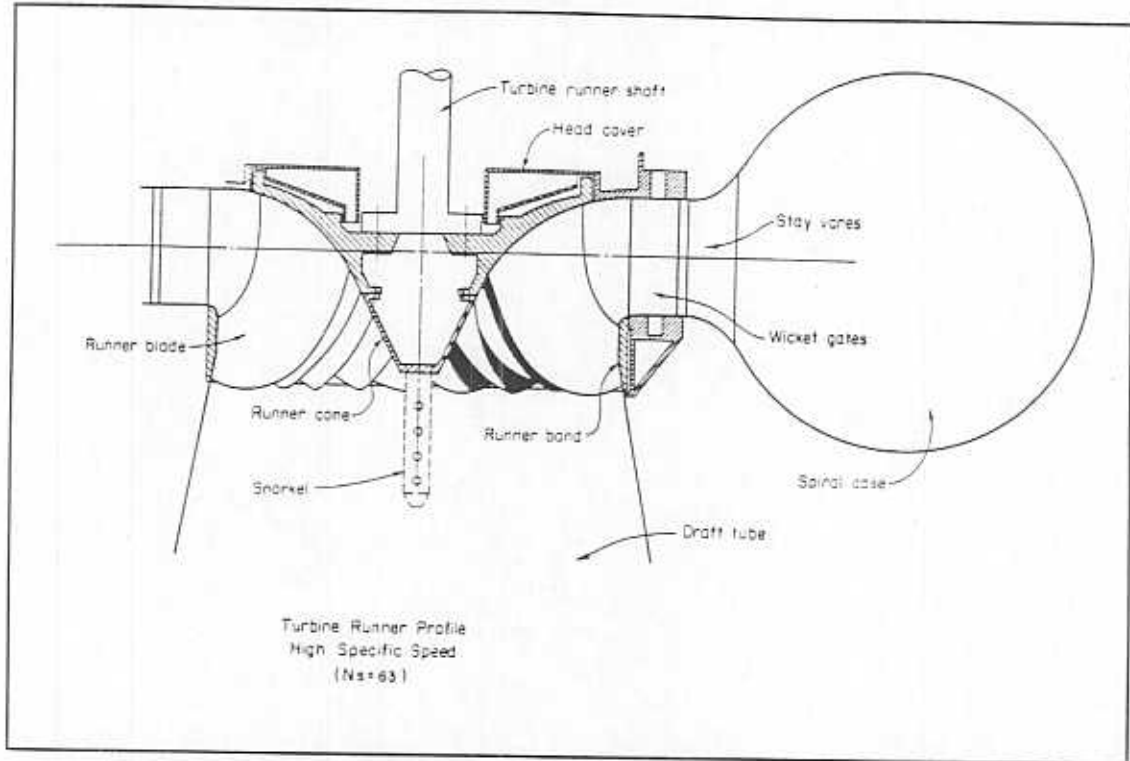


Figure 1-1. Hydraulic turbine components (after Falvey, 1971, Figure 4).

The ability of the draft tube surge to influence the hydraulic, structural, mechanical, and electrical systems of a power plant makes it imperative that the nature of possible excitations be clearly understood, over the full range of operating conditions. This allows the design of other components to be carried out with consideration for the possible problems due to draft tube surging.

Dimensional analysis indicates that the frequency and amplitude of draft tube surge pressure pulsations are functions of a dimensionless swirl parameter, the Reynolds number, and the draft tube length to diameter ratio. Research using air flow through model draft tubes has confirmed this functional relationship and has shown that viscous effects are negligible at the high Reynolds numbers encountered

in prototype and model hydraulic turbines. The objective of this project was to extend this research by studying the draft tube surge in a complete hydraulic model of a turbine and draft tube; the model was operated over a large region of the turbine hill curve. The hypothesis was that for a given draft tube shape, all points on the turbine hill curve having the same swirl parameter would exhibit the same surging behavior. To test this hypothesis, attempts were made to relate the dimensionless parameters of the surge to the dimensionless swirl parameter. Parameters were mapped on to the turbine hill curve to identify regions where anomalies existed.

The term *swirl* is used to describe a flow containing both axial and rotational components of velocity. Under optimum conditions the flow leaving a turbine runner is essentially axial, with no rotational velocity component and no swirl. However, when the turbine must operate away from the optimum condition, swirling flow occurs. When power output is lower than optimum, the flow leaving the runner rotates in the same direction as the runner; the swirl is said to be positive. If the power output is greater than optimum, the flow leaves the runner in an opposite direction to the runner rotation, and the swirl is negative.

As the absolute value of swirl in the draft tube increases, the axial velocity distribution in the draft tube becomes distorted. The flow becomes concentrated around the outside edge of the tube. The onset of draft tube surging occurs when, at a critical level of swirl, the flow along the center line of the draft tube reverses, and a helical vortex forms around the periphery of the reverse flow region. The helix tends to rotate around the axis of the draft tube; this motion is described as the *precession* of the vortex. The formation of the helical vortex has been termed a *vortex breakdown* in the fluid mechanics literature.

If the pressure in the draft tube is low enough, the pressure within the vortex core will drop to the vapor pressure, causing cavitation to occur, and making the vortex visible. Air injected into the draft tube can also make the vortex visible. The form and appearance of the helical vortex has inspired the use of additional descriptive terms such as *spiral vortex*, *corkscrew vortex*, and *vortex rope*. Figure 1-2 shows a typical helical vortex.

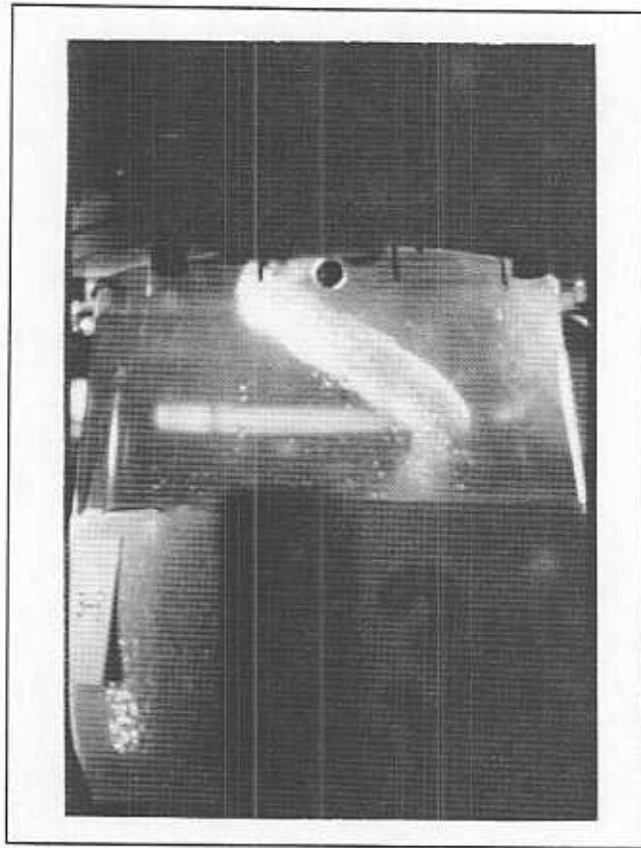


Figure 1-2. Helical vortex in draft tube surging region. This photo of a cavitated vortex core was taken on Run 3-8.

Unsteady flows similar to the draft tube surge have also been observed in other environments with combined axial and rotational flow, including the flow over delta wings with highly swept leading edges. Adverse effects include changes in the lift, drag, and moment curves of the wing. Figure 1-3 shows the vortex breakdown in the flow over a delta wing.

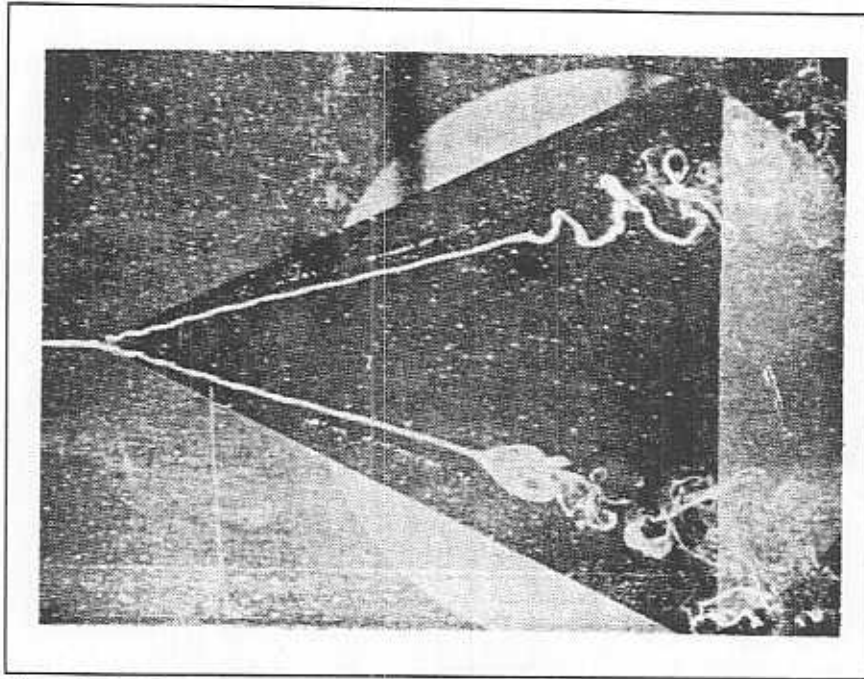


Figure 1-3. Vortex breakdown in the flow over a highly swept delta wing (after Leibovich, 1984, Figure 1).

The dominant characteristic of the surge is the pressure fluctuation that occurs as a result of the vortex precession. The center of the vortex is a zone of low pressure. Consequently, a low pressure is detected at the draft tube wall with each passage of the vortex. Palde (1974) notes that the presence of a hollow vortex core, either due to cavitation or air, is not necessary for draft tube surging to occur; cavitation or air only makes the vortex visible.

The pressure fluctuations in the draft tube can in turn excite other portions of the hydraulic or structural system. Problems associated with draft tube surging include severe vibrations, fatigue failures, noise, pressure fluctuations within the penstock and draft tube, power swings, and excessive axial movement and runout of the turbine runner and shaft. Numerous techniques have been examined for reducing these effects, with success varying widely. At many sites operations have been prohibited in the most severe surge regions (Falvey, 1989).

Repeated reference is made to the turbine hill curve as a means of visualizing the operational characteristics of the model turbine. Figure 1-4 shows the hill curve for the model turbine used in this study. Efficiency contours are plotted on the space defined by the speed ratio and unit power, two fundamental parameters used in model studies of hydraulic turbines. The speed ratio is a non-dimensionalized ratio of runner speed to net head. Thus, either increasing the speed or decreasing the head causes the speed ratio to increase. The unit power relates the output power to the net head, so that increasing power output at the same head causes an increase in the unit power. This same plotting space was used to map the dimensionless parameters describing the draft tube surge.

An extensive literature search revealed only one study considering surge behavior over wide ranges of the turbine hill curve (Hosoi, 1965). In this study, the amplitude and frequency of pressure fluctuations were recorded over the full operating range of a model turbine, but the dimensionless swirl parameter was not considered in the analysis.

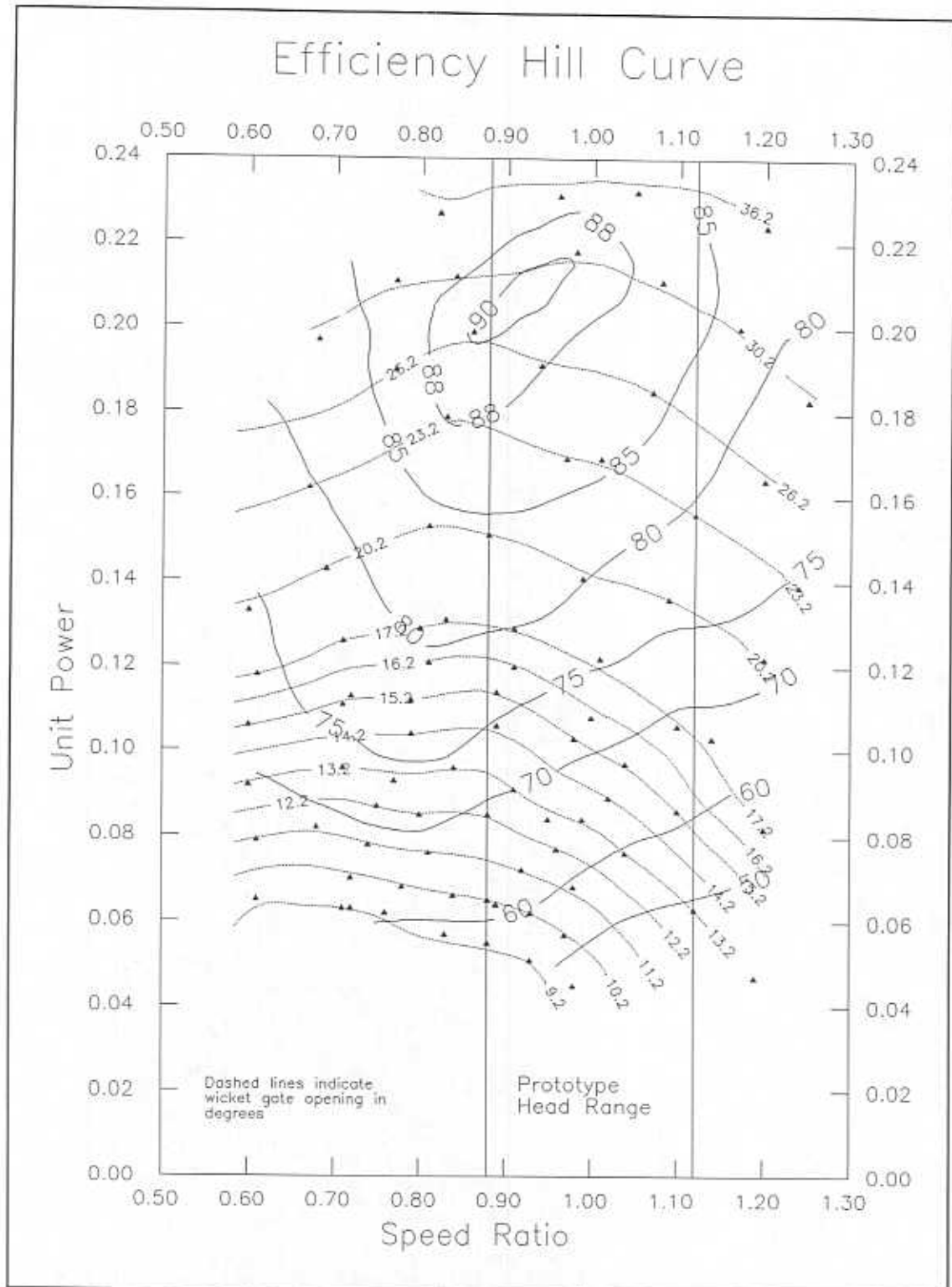


Figure 1-4. Turbine efficiency hill curve. Solid contours are lines of constant efficiency (percent). Lines of constant wicket gate opening are shown as dotted lines. Vertical lines at speed ratios of 0.88 and 1.12 indicate the prototype operating range. Full gate opening for the prototype is 34°. The wicket gates are fully closed at 0°.

CHAPTER 2

LITERATURE REVIEW

The literature applicable to the draft tube surging problem comes from a number of disciplines, including fluid mechanics, aerodynamics, and hydraulics. A great deal of the literature comes from work done by the U. S. Bureau of Reclamation (USBR) in connection with the design of the Grand Coulee Third Power Plant, part of the USBR's Columbia Basin Project. One especially useful item was a review report and annotated bibliography prepared by Falvey (1971).

The available literature can be divided into several classes. These include field experiences with draft tube surging and its effects, analysis of the vortex breakdown as a general flow phenomenon, and modeling of the draft tube surge.

2.1 GENERAL OVERVIEW AND CLASSIFICATIONS OF SURGING

The occurrence of draft tube surging in fixed blade reaction turbines, most usually of the Francis type, has been known since early in this century. The first analytical study of draft tube surging and the problems associated with it was offered by Rheingans (1940). Rheingans provided evidence that the large power swings observed in some reaction turbines at part load or overload were directly related to the presence of pressure fluctuations in the draft tube, accompanied by an audible *swish* emanating from the tube at the same frequency as the power swing. Rheingans found that the frequency of pressure fluctuations and power swings was given empirically by:

$$f_{\text{surge}} = \frac{f_{\text{shaft}}}{3.6} \quad (2-1)$$

where:

f_{shaft} = rotational frequency of the turbine runner and shaft

Subsequent investigations (Dériaz, 1960) using transparent draft tube models showed that the flow in surging regions contains a helical vortex that precesses about the axis of the draft tube at approximately the frequency given by Eq. (2-1). In a hydraulic turbine the vortex may be filled with water, air, or water vapor.

It is well accepted that the undesirable effects of draft tube surging originate from the pressure field associated with the precessing helical vortex. The fluctuating pressures provide an excitation that can interact with hydraulic, structural, mechanical, or electrical components of the turbine and power plant. Pressure fluctuations within the draft tube tend to produce a fluctuating head on the turbine, which in turn produces fluctuations in discharge, torque, and output power. Rheingans showed that extremely large power swings could be produced if the output power fluctuations occurred at or near the natural frequency of the generator connected to the power system. In addition, severe pressure fluctuations can occur in the penstock when discharge and head fluctuate at the natural frequency of the penstock. Even in situations where resonance is not a problem, draft tube surging can cause excessive vibrations, noise, cavitation, and axial movement of the turbine runner and shaft.

2.1.1 Asynchronous Surging

Two types of pressure fluctuations associated with the draft tube surge are identified in the literature. The first is an *asynchronous* pressure fluctuation due to the precession of the helical vortex about the axis of the draft tube. A pressure transducer located at a point on the draft tube wall will detect a reduction in pressure each time the vortex passes the transducer. A transducer mounted 180° opposite will

experience the same pressure fluctuation directly out of phase with the first transducer. A purely asynchronous fluctuation is a local effect of the vortex motion; it does not produce a fluctuation in the average pressure at a given cross section along the axis of the draft tube. Despite this fact, even a purely asynchronous surge can cause excessive noise and vibrations.

2.1.2 Synchronous Surging

The second type of fluctuation is a *synchronous* fluctuation in which the average pressure at a given cross section along the draft tube axis varies with time. In this case, transducers mounted on opposite walls of the draft tube should be in phase. This type of fluctuation has the greatest potential for influencing other portions of the system. As the average pressure within the draft tube changes, the net head across the runner also varies, leading to discharge and power fluctuations. Superposition of synchronous and asynchronous components is possible (Fanelli, 1989).

Several theories have been advanced to account for the presence of synchronous pressure fluctuations. Dériaz (1960) proposed that the interaction of the vortex with piers in the draft tube foot could induce a synchronous pressure pulsation. As the vortex moves within the draft tube it is alternately aligned with either the flow passages or the piers. This could produce a fluctuating discharge coefficient for the foot of the draft tube and thereby produce a fluctuating discharge and fluctuating head. Fanelli (1989) proposed that interaction between the helical vortex and the draft tube elbow produces synchronous fluctuations. The presence of a cavitating vortex core (i.e., a two-phase flow) has also been considered as a requirement for synchronous surging. Nishi et al. (1980), conducted a model study in which the presence of a cavitating vortex core produced large synchronous pressure pulsations. Other investigators have made contradictory observations. Cassidy and

Falvey (1970) observed synchronous pulsations in straight tubes with air as the working fluid. Palde (1974) found that the presence of a cavitated vortex core had little effect on the amplitude of observed pressure fluctuations. Mollenkopf and Raabe (1970) observed that the frequency and amplitude of pressure fluctuations due to draft tube surging was independent of the cavitation coefficient σ , as long as σ remained above the critical level at which turbine efficiency begins to drop.

2.2 FIELD EXPERIENCES

A number of authors have reported case studies of field experiences with draft tube surging problems. Fluctuation of penstock pressure is one of the more common problems. Kito (1959) described a Japanese power plant with severe vibrations of the penstock caused by draft tube surging. Attempts to control the surge itself caused large reductions in output power. The problem was finally solved by adding stiffener rings to the penstock walls and allowing surging to continue. This plant was especially susceptible to draft tube surging because it was not only required to operate under varying head and load conditions, but also at two different speeds corresponding to 50 Hz and 60 Hz power output.

Guarga, Hiriart, and Torres (1983) reported that at the La Angostura power plant in southeastern Mexico, pressure fluctuations in the penstocks induced by draft tube surging were as high as 60.5 m peak-to-peak compared with a total head of 104 m. This problem was solved using a very small flow of air injected into the draft tube through the runner cone. The maximum penstock pressure fluctuation was reduced to 7.7 m.

Falvey (1989) described a problem with the USBR's Fremont Canyon Power Plant. Vibrations and noise due to surging were so severe that operation was prohibited in the surging zone. A variety of air admission schemes and structural changes to the draft tube were attempted, with unsatisfactory results. Finally, it was

found that the exit area of the runner was significantly smaller than most runners of similar specific speed. The trailing edge of each runner blade was trimmed to increase the exit area. This produced an increase in maximum power output and reduced the size and severity of the surge region considerably.

2.3 REMEDIAL MEASURES

Grein (1980) summarized field methods used in attempts to reduce or eliminate surging and its effects. Among the methods most commonly used are air injection in the runner and draft tube area, structural modifications to the draft tube, and occasionally modifications to the runner. Each of these usually introduces some loss of efficiency. The variations on these approaches seen in the field are nearly as numerous as the number of field problems, as each situation is unique. Bhan, Codrington, and Mielke (1988), in a survey of twenty-one different cases, note that, "In general, no single solution can be guaranteed to eliminate draft tube surge problems."

2.3.1 Air Admission

Often the first attempt at reduction of draft tube surging problems involves the admission of air into the draft tube. Air is commonly supplied just below the runner, at the draft tube inlet. On some units provisions are made for admitting air through the runner head cover, through the runner cone, or through a snorkel attached to the runner cone. In some cases air can naturally flow into the draft tube during operation at low tailwater. However, at high tailwater, or on units that are set quite low for cavitation protection, compressed air must be injected into the draft tube.

Grein (1980) reports that in most cases large amounts of air, up to 3 percent of turbine discharge, are required to achieve significant reduction of pressure pulsations. These large volumes of air cause significant efficiency loss and require a large power expenditure for the compressor.

Ulith (1968), in tests on a model turbine, found that the most effective location for injection of compressed air was the annular space between the wicket gates and the runner inlet. At this location only 0.08 percent air flow was required to achieve a satisfactory cushioning effect. Additionally, air injection at this location did not cause any reduction in efficiency.

2.3.2 Structural Modifications

Common structural modifications to the draft tube are discussed by Falvey (1971) and Grein (1980). The most common structural modification is the addition of a flow straightener in the draft tube that serves to break up the vortex. Typical devices include fins attached to the draft tube wall, or concentric cylinders mounted in the draft tube. Fins have proven to be effective in many cases, but they introduce significant efficiency loss and are also subject to cavitation erosion and structural vibrations. Concentric cylinders do not normally reduce efficiency significantly. However, structural problems with mounting the cylinders in the draft tube are significant. Cavitation erosion and vibration are also serious problems. One advantage of concentric cylinders is that the supporting struts can also serve as air injection locations. This may help reduce the surge further and prevent cavitation damage to the struts.

Another type of modification is an extension to the runner cone, sometimes called a snorkel. These devices may be attached to the runner, or fixed within the draft tube so that they sit just beneath the runner cone. Some authors suggest that these devices break up the surge by filling a portion of the reverse flow region (e.g., Grein, 1980). Air injection can also be combined with these structures. When attached to the draft tube the disadvantages are similar to those for concentric cylinders. If attached to the runner, these devices may cause excessive runout of the shaft due to lateral forces arising from pressure pulsations in the draft tube.

One modification that has been studied experimentally, but never installed on a prototype unit, is a bypass to carry flow from the penstock or spiral case, and inject it into the draft tube in an opposite direction to the swirl (Seybert, Gearhart, and Falvey, 1978; Gearhart, Yocum, and Seybert, 1979). Studies were performed to estimate the bypass flow required to affect the surge in the Grand Coulee Third Power Plant 600 MW turbines. Elimination of the surge required bypass flows of 10 to 13 percent of the total turbine discharge, depending on the value of the swirl parameter. Significant reduction of pressure fluctuations could be realized with smaller bypass flows.

2.4 VORTEX BREAKDOWN

The flow phenomenon associated with draft tube surging has been described in the fluid mechanics literature as a vortex breakdown. This term was first applied to the flow occurring over highly swept delta wings. At large angles of attack a vortex forms on the upper surface of such wings, just behind the leading edge of the airfoil. On highly swept wings, the flow in this vortex also contains a significant velocity component directed along the axis of the vortex. Under some conditions, the vortex suddenly breaks down into the spiraling flow, seen previously in Figure 1-3. In this case, the swirling flow is unconfined, whereas the flow in a turbine draft tube is confined. Notable observations of the vortex breakdown phenomenon in confined flows were provided by Harvey (1962) and Sarpkaya (1971).

The vortex breakdown has been found to coincide with the formation of a stalled or reversed flow region along the axis of the flow (Nishi et al., 1982). As the swirl in the flow increases, the axial velocity is reduced at the centerline of the tube and increased near the walls. At a critical swirl level, a sudden transition in the flow is observed. A region of stalled or reversed flow is developed in the center of the flow, and a helical vortex forms around the reversed flow.

2.4.1 Vortex Structure

If the swirl is clockwise looking downstream, the helical vortex takes the form of a left handed screw. The precession of the vortex is in the same direction as the swirl. The helical vortex can be visualized as the rolling up of a shear layer forming at the boundary between the reverse flow region and the surrounding swirling flow. This produces a vortex rope that is oriented everywhere perpendicular to the swirling flow surrounding the reverse flow region (Nishi et al., 1982). Thus, as the swirl increases, the pitch of the vortex can be expected to increase.

The most common flow structure associated with the vortex breakdown is a single helical vortex. However, Sarpkaya (1971), in experiments with a diverging tube, also observed a double vortex at low Reynolds numbers (1000 to 2000). The two spirals were intertwined together within the tube, 180° opposite one another.

Escudier and Zehnder (1982) also observed the double spiral in straight, diverging tubes. The double spiral seemed to be very unstable, and alternately was replaced by a single spiral. Other references to the existence of a double spiral have been made by Nishi et al. (1982), and Fanelli (1989).

2.4.2 Hydraulic Jump Analogy

The vortex breakdown has been likened by some investigators to the familiar hydraulic jump observed in open channel flow. Benjamin (1962, 1965) presents a mathematical justification for this analogy. The vortex breakdown is seen as a transition from a supercritical flow that can not support an axisymmetric standing wave to a subcritical flow that can support such a wave. A purely axial flow is infinitely supercritical.

Specifically, the vortex breakdown is thought to be analogous to a weak, undular hydraulic jump. In this type of jump there is very little dissipation of energy.

Benjamin and Lighthill (1954) showed that the formation of standing waves on the downstream side of such a jump reduces the downstream flow force enough to match the upstream conditions, without producing a large energy loss.

The helical vortex is analogous to the standing wave formed on the downstream side of an undular jump. As the swirl in the flow is increased the flow becomes less supercritical. When the flow reaches a slightly supercritical state, vortex breakdown occurs, producing a subcritical flow that contains the helical vortex.

2.5 MODEL-PROTOTYPE SIMILARITY

In the late 1960's the USBR began studying draft tube surging in connection with the proposed Grand Coulee Third Power Plant. Efforts were made to develop methods for modeling the phenomenon in the laboratory and then transferring the results to prototype installations. The approach taken was to view the draft tube surge as a gross flow phenomenon, depending on the gross geometric and operating characteristics of the turbine and draft tube.

Dimensional analysis showed that five dimensionless parameters were relevant to the draft tube surging problem (Cassidy, 1969). The non-dimensional frequency and pressure parameters were each a function of three other dimensionless parameters: (1) the momentum parameter of the flow entering the draft tube (hereafter referred to as the swirl parameter); (2) the Reynolds number (in terms of axial velocity); and (3) the length to diameter ratio of the draft tube. The basic equations for calculating the draft tube swirl parameter for an operating turbine were also presented.

2.5.1 Air Model Tests

Tests were conducted to evaluate the applicability of the dimensionless parameters (Cassidy, 1969; Cassidy and Falvey, 1970; Falvey and Cassidy, 1970). The tests were conducted on a variety of cylindrical, diverging, and elbow type tubes,

using air as the working fluid. It was assumed that only the value of the swirl parameter was important, not the manner in which swirl was introduced. Thus, to simplify the experiments, swirl was introduced using vanes similar to the wicket gates of a hydraulic turbine; the models did not include a runner.

The absence of a runner meant that each setting of the wicket gates corresponded to a unique value of the swirl parameter. In contrast, in a hydraulic turbine with both wicket gates and a runner, many different values of the swirl parameter can be obtained at each wicket gate setting, and identical swirl values can be obtained at different wicket gate settings.

Three conclusions were drawn from the study: (1) surging occurs above a critical absolute value of the draft tube swirl parameter; (2) the frequency and amplitude of pressure fluctuations is independent of viscous effects for Reynolds numbers above about 80,000; (3) for a given draft tube geometry, the frequency and pressure parameters could be correlated to the draft tube swirl parameter.

Palde (1972) conducted extensive experiments with model draft tubes of various shapes including cylindrical, diverging, and elbow type. These experiments were again conducted with air as the working fluid and with swirl introduced by vanes only. The testing showed that the shape has a significant influence on the frequency and amplitude of pressure fluctuations, and the range of swirl values over which surging will occur. Straight tubes in general had higher frequency and higher amplitude surges and experienced surging over a wider range. The throat geometry was found to have more influence than elements further downstream; the divergence of the throat was the most important parameter.

Nystrom (1982) and Nystrom and Bozoian (1983) examined the effect of downstream geometry on the frequency and amplitude of pressure fluctuations due to draft tube surging. Tests conducted with an air model showed that downstream geometry was not a significant factor. This result was consistent with the

observations of Palde (1972) that inlet conditions of the draft tube had far greater effect than downstream elements. The tests did point out the fact that resonance within either the test setup or the prototype can have a major impact on pressure amplitudes. This is emphasized by the case of the La Angostura Power Plant described earlier (Guarga, Hiriart, and Torres, 1983). In that case draft tube surging caused enormous penstock pressure fluctuations, which were greatly reduced by the admission of air into the draft tube. However, the problem could not even be reproduced using a scale hydraulic model.

2.5.2 Hydraulic Model Tests

Palde (1972) reported on the comparison of air model (no runner) and hydraulic model tests of the Grand Coulee Pumping Plant pump-turbine draft tubes. In each test, frequency and pressure parameters were related to the draft tube swirl parameter. Comparison of the frequency parameters obtained in the two tests were quite good. The comparison of pressure parameters was less convincing; however, reasonable correlation with the air model tests was provided by the hydraulic model tests performed at high tailwater levels.

The construction of the Third Power Plant at Grand Coulee Dam produced unique opportunities for studying the draft tube surging problem. In addition to Grand Coulee, two other power plants (Marimbondo, Brazil; Cerron Grande, Salvador) were constructed at about the same time using nearly homologous turbine and draft tube designs. Hydraulic model tests were conducted for turbines in all three plants. Fisher, Palde and Ulith (1980) compared the results of eleven different series of draft tube surging data obtained from these models and prototype units. Test data were obtained for seven different model configurations including two model sizes and both once-through and closed-loop test stands. Also, four different prototype data series were obtained. The comparison showed that the draft tube

surge was not sensitive to the individual characteristics of the test stand, and that there was good correlation between all of the data sets. The conclusion was that prototype pressure fluctuations could be predicted from model test results if pressure fluctuations were not in resonance with other portions of the system.

CHAPTER 3

THEORETICAL CONSIDERATIONS

3.1 DIMENSIONAL ANALYSIS

Dimensionless parameters of the draft tube surge based on gross flow variables were first presented by Cassidy (1969) and later modified by Falvey and Cassidy (1970). Two properties of the surge, the frequency, f , and the root-mean-square (rms) amplitude of the pressure fluctuation, $\sqrt{(p')^2}$, were of interest. These two quantities were assumed to be functions of the density, ρ , the viscosity, ν , the draft tube throat diameter, D_3 , the length of the draft tube, L , the discharge, Q , and the flux of angular momentum, Ω . The assumed functional relationships are:

$$f = \psi_1(\rho, \nu, D_3, L, Q, \Omega) \quad (3-1)$$

$$\sqrt{(p')^2} = \psi_2(\rho, \nu, D_3, L, Q, \Omega) \quad (3-2)$$

Dimensional analysis simplifies these relationships to:

$$\frac{f D_3^3}{Q} = \psi_3\left(\frac{\Omega D_3}{\rho Q^2}, \frac{L}{D_3}, \frac{4Q}{\pi D_3 \nu}\right) \quad (3-3)$$

$$\frac{D_3^4 \sqrt{(p')^2}}{\rho Q^2} = \psi_4\left(\frac{\Omega D_3}{\rho Q^2}, \frac{L}{D_3}, \frac{4Q}{\pi D_3 \nu}\right) \quad (3-4)$$

where:

$\left(\frac{f D_3^3}{Q}\right)$ = frequency parameter of draft tube pressure pulsation

$\left(\frac{D_3^4 \sqrt{(p')^2}}{\rho Q^2}\right)$ = pressure parameter of draft tube pressure pulsation

$\left(\frac{\Omega D_3}{\rho Q^2}\right)$ = draft tube swirl parameter (momentum parameter)

$\left(\frac{L}{D_3}\right)$ = draft tube length to diameter ratio

$\left(\frac{4Q}{\pi D_3 \nu}\right)$ = Reynolds number expressed in terms of discharge

The frequency and pressure parameters are functions of the draft tube swirl, the draft tube length to diameter ratio, and the Reynolds number.

Initial work by Cassidy (1969) with a draft tube model using air as the working fluid established that the frequency and pressure parameters are independent of viscous effects for Reynolds numbers above about 80,000. The Reynolds number for prototype units and even small hydraulic models is much greater than 80,000. Thus, for a given draft tube shape (assuming that $\left(\frac{L}{D_3}\right)$ is defined by the shape), the frequency and pressure parameters depend only on the swirl parameter.

3.2 CALCULATION OF THE SWIRL PARAMETER

The draft tube swirl parameter is a non-dimensionalized ratio of angular momentum flux to linear momentum flux. The angular momentum flux appears in the numerator, along with an additional length term; the linear momentum flux in the denominator is multiplied by an area term.

Cassidy (1969) outlined the calculation of the swirl parameter for an operating turbine. This development will be presented here.

The swirl parameter can be calculated from knowledge of the runner diameter, wicket gate setting and geometry, and performance characteristics of the turbine. Point 1 is defined to be directly upstream of the runner, as the flow exits the wicket gates. Point 2 is at the downstream side of the runner, as the flow enters the draft tube. The derivation begins with the basic equation for power output from the turbine:

$$P = \omega T \quad (3-5)$$

where:

P = turbine output power

ω = angular velocity

T = torque

The torque is given by: $T = \Omega_1 - \Omega_2$ (3-6)

where:

$\Omega_1 - \Omega_2 =$ change of angular momentum flux across the runner

Substituting the expression for torque into Eq. (3-5) produces:

$$\frac{P}{\omega} = \Omega_1 - \Omega_2 \quad (3-7)$$

Multiplying each of the terms of Eq. (3-7) by $(D_3/\rho Q^2)$ and rearranging terms yields:

$$\frac{\Omega_2 D_3}{\rho Q^2} = \frac{\Omega_1 D_3}{\rho Q^2} - \frac{P D_3}{\omega \rho Q^2} \quad (3-8)$$

The left side of Eq. (3-8) is the draft tube swirl parameter. The first term on the right is the swirl parameter for the flow leaving the wicket gates and entering the runner. This term is referred to as the *wicket gate momentum parameter*. The second term on the right is the swirl extracted from the flow by the turbine runner. Note that for a model having only wicket gates, the draft tube swirl parameter is equal to the wicket gate momentum parameter.

3.2.1 Wicket Gate Momentum Parameter

Two methods for determining the wicket gate momentum parameter appear in the literature. The first is a graphical technique, described by Cassidy (1969). The second technique uses a potential flow solution for the flow through the wicket gates. The second technique is widely accepted as the more accurate method, and was the technique used for this project. A discussion of both procedures is presented here to aid in the understanding of the wicket gate momentum parameter.

3.2.1.1 Graphical Analysis

The graphical technique is based on the assumption that the flow is perpendicular to the location of minimum cross section between adjacent wicket gates, and that the velocity is uniform across the minimum cross section.

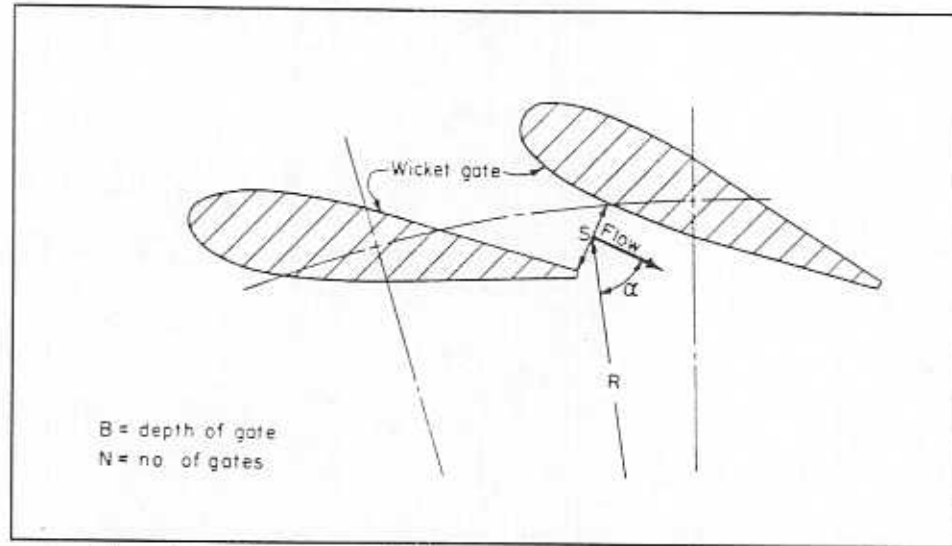


Figure 3-1. Wicket gate definition sketch (after Palde, 1972, Figure 1).

The technique is defined in terms of the gate layout shown in Figure 3-1. B is the depth of the gate, N is the number of gates, and S is the minimum distance between the gates for a given gate opening. Values of R , S , and α can be determined for a particular gate setting from gate layout drawings or measured from the actual gates. The flux of angular momentum for N gate openings is given by:

$$\Omega_1 = N \rho q V R \sin(\alpha) = \frac{N \rho q^2 R \sin(\alpha)}{\alpha} \quad (3-9)$$

where:

q = discharge through a single gate passage

α = flow area of one gate passage

V = velocity of flow between gates

Noting that Nq is the total discharge Q , Eq. (3-9) can be rewritten as:

$$\Omega_1 = \frac{\rho Q^2 R \sin(\alpha)}{A} \quad (3-10)$$

where:

A = total flow area for N gates

Multiplying by $(D_3/\rho Q^2)$ and noting that the total flow area for N gates of height B is BNS , the wicket gate momentum parameter is given by:

$$\frac{\Omega_1 D_3}{\rho Q^2} = \frac{D_3 R \sin(\alpha)}{BNS} \quad (3-11)$$

The wicket gate momentum parameter is thus a function of only the gate opening.

3.2.1.2 Potential Flow Analysis

The assumption of perpendicular flow through the minimum cross section of the gate opening is a major one, especially for cambered gates. To improve upon the graphical procedure, a potential flow analysis procedure was developed (Yocum, 1978). The radial wicket gate layout is converted to a linear cascade. An existing computer program known as the Douglas-Neumann Cascade Program is then used to analyze the potential flow through the wicket gates. This result is then used to compute the wicket gate momentum parameter. The procedure was used to analyze the flow through non-cambered wicket gates, and results were confirmed by velocity measurements made on a model wicket gate layout with air as the working fluid. The potential flow solution was found to vary only slightly from the results of the graphical procedure.

Similar tests using cambered wicket gates (Gearhart, Yocum, and Seybert, 1979) indicated a larger difference between the potential flow and graphical procedures, and confirmed that the potential flow procedure was the most accurate.

The potential flow method was used by the USBR to evaluate the wicket gate momentum parameter for the cambered gates of the Allis-Chalmers, 9-inch model turbine (personal communication, Brent Mefford, USBR, Denver, Colorado). The analysis showed that the wicket gate momentum parameter was given by the equation:

$$\frac{\Omega_1 D_3}{\rho Q^2} = 59 (GO)^{-1.18} \quad (3-12)$$

where:

GO = gate opening in degrees, measured from 0° when fully closed

Figure 3-2 shows the value of the wicket gate momentum parameter as a function of the gate opening.

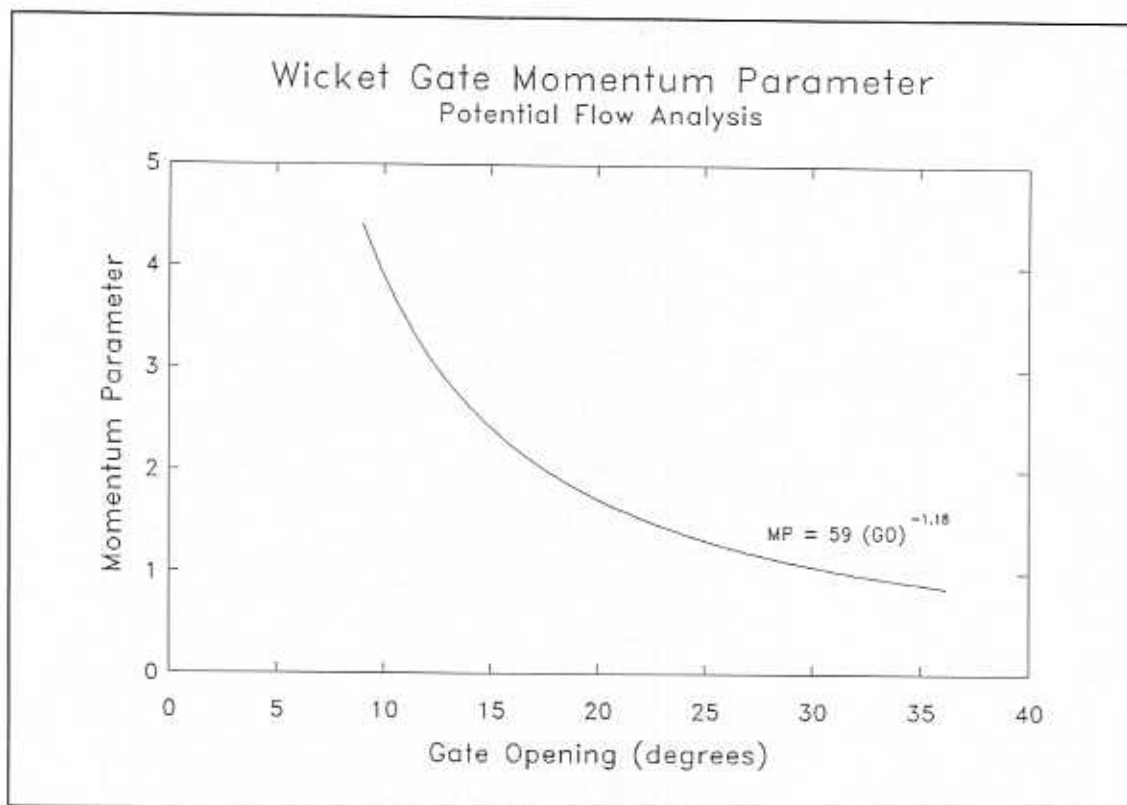


Figure 3-2. Wicket gate momentum parameter.

3.2.2 Swirl Extracted by the Runner

The swirl extracted from the flow by the turbine runner is given by the second term on the right of Eq. (3-8):

$$\frac{P D_3}{\rho \omega Q^2} \quad (3-13)$$

Falvey and Cassidy (1970) developed a modification of this term that leads to some useful conclusions. The modification expresses Eq. (3-13) in terms of the speed ratio ϕ_z , unit power, HP_{11} , and unit discharge, Q_{11} :

$$\phi_z = \frac{\pi N D_2}{60 \sqrt{2gH}} \quad (3-14)$$

$$HP_{11} = \frac{(BHP)}{D_2^2 H^{3/2}} \quad (3-15)$$

$$Q_{11} = \frac{Q}{D_2^2 H^{1/2}} \quad (3-16)$$

where:

BHP = turbine output (brake horsepower)

D_2 = throat diameter of the turbine runner

H = net head on the turbine

N = runner rotational speed

g = acceleration of gravity

Substituting each of these parameters into Eq. (3-13), converting output power from horsepower to ft-lb/sec, and rearranging yields:

$$\begin{aligned} \frac{P D_3}{\rho \omega Q^2} &= \frac{[550(HP_{11}) D_2^2 H^{3/2}] D_3}{\rho \left(\frac{2\pi N}{60} \right) (Q_{11} D_2^2 H^{1/2})^2} \\ &= \frac{550(HP_{11}) H^{1/2} D_3}{\rho \left(\frac{2\pi N}{60} \right) Q_{11}^2 D_2^2 \left(\frac{\sqrt{2g}}{\sqrt{2g}} \right)} \\ &= \frac{550}{2\rho \sqrt{2g}} \frac{(HP_{11}) D_3}{\left(\frac{\pi N D_2}{60 \sqrt{2gH}} \right) D_2^2 Q_{11}^2} \\ &= \left(\frac{550}{2\rho \sqrt{2g}} \right) \left(\frac{HP_{11}}{Q_{11}^2 \phi_z} \right) \left(\frac{D_3}{D_2} \right) \end{aligned} \quad (3-17)$$

The significance of this result is that the swirl extracted by the turbine depends entirely on constants, the fixed geometry of the runner and draft tube, and the turbine parameters ϕ_2 , HP_{11} , and Q_{11} . For a given gate setting and value of ϕ_2 , HP_{11} and Q_{11} are known from the hill curve. (The ratio of Q_{11} to HP_{11} defines the efficiency). In addition, the wicket gate momentum parameter is a function of only the wicket gate opening. Thus, the draft tube swirl parameter is independent of the absolute value of head and discharge; it is defined exactly for each point on the hill curve.

3.3 APPLICATION TO PROTOTYPE INSTALLATIONS

Application of model test results to prototype installations is achieved by equating the pressure and frequency parameters of the model to those that would exist in the prototype at the same value of draft tube swirl. The necessary equations are as follows, with m denoting the model and p the prototype.

Given that the draft tube swirl values are equal:

$$\left(\frac{\Omega_2 D_3}{\rho Q^2} \right)_m = \left(\frac{\Omega_2 D_3}{\rho Q^2} \right)_p \quad (3-18)$$

the pressure and frequency parameters must also be equal.

$$\left(\frac{D_3^4 \sqrt{(p')^2}}{\rho Q^2} \right)_m = \left(\frac{D_3^4 \sqrt{(p')^2}}{\rho Q^2} \right)_p \quad (3-19)$$

$$\left(\frac{f D_3^3}{Q} \right)_m = \left(\frac{f D_3^3}{Q} \right)_p \quad (3-20)$$

Thus, the prototype pressure fluctuation and its frequency are given by:

$$\left(\sqrt{(p')^2} \right)_p = \left(\frac{D_3^4 \sqrt{(p')^2}}{\rho Q^2} \right)_m \left(\frac{\rho Q^2}{D_3^4} \right)_p \quad (3-21)$$

$$f_p = \left(\frac{f D_3^3}{Q} \right)_m \left(\frac{Q}{D_3^3} \right)_p \quad (3-22)$$

An example calculation of prototype frequency and amplitude using model test results is given in Appendix B.

It is important to reiterate that dimensional analysis indicates that for draft tubes of the same shape, operating at high Reynolds numbers, the frequency and pressure parameters are functions of only the swirl parameter. The actual operating point (position on the turbine hill curve) of the prototype need not correspond with the operating point of the model. If the swirl parameters are equal, the dimensionless parameters defining the pressure fluctuation should be equal.

CHAPTER 4

EXPERIMENTAL EQUIPMENT AND PROCEDURES

4.1 TEST FACILITY

The model turbine used for the project is a homologous, 1:40.3 scale model of the 700 MW Allis-Chalmers turbines (units G22, G23, and G24) installed at Grand Coulee Third Power Plant, on the USBR's Columbia Basin Project. The test facility provides geometric similarity with the prototype installation from the penstock intake to the downstream tailrace. The model turbine was built by Allis-Chalmers as required by the contract for the units installed at Grand Coulee Third Power Plant. Following testing by Allis-Chalmers in their closed-loop test facility at York, Pennsylvania, the model was installed in the USBR's model turbine test stand at Estes Power Plant, Estes Park, Colorado. In 1988 the USBR test stand was decommissioned and moved to the Hydromachinery Laboratory of the Department of Civil Engineering at Colorado State University.

The model is installed in a once-through system drawing water directly from Horsetooth Reservoir, located immediately west of the laboratory. The model was originally designed to operate in the prototype range of 220-355 ft of head. As installed at the Hydromachinery Laboratory, the maximum available head is about 250 ft. Horsetooth Reservoir provides irrigation and municipal water to Fort Collins and surrounding areas, and thus experiences a significant drawdown during the summer and late fall months. During the time these tests were performed, the maximum available head was about 170 ft.

Water is delivered from Horsetooth Reservoir to the test facility by 5500 ft of 36-inch diameter steel pipe. Immediately before entering the laboratory, the pipeline reduces to 24-inch diameter. Inside the laboratory an 18-inch diameter pipeline carries the flow to the model. Downstream, a butterfly valve is used to apply back pressure on the model. The butterfly valve is located just downstream of a 25-ft high standpipe.

The model elbow type draft tube is constructed of fiber glass, with a clear plastic throat section to allow observation of the flow. The model is equipped with air injection ports in the runner crown, just upstream of the trailing edges of the runner buckets. Air injection was used for flow visualization at some test points.

The test facility is operated from a control room located on the second floor of the laboratory. Load is placed on the turbine by a water cooled, eddy current, absorption dynamometer. The dynamometer control console provides for both load and speed control of the unit.

The operating status of the test facility and the model turbine is monitored by an HP85 computer and HP3421A Data Acquisition and Control Unit. The computer collects data from pressure transducers, thermocouples, a tachometer, and the dynamometer torque load cell.

4.2 EXPERIMENTAL PROCEDURE

The basic experimental procedure was to operate the turbine model at test points throughout the draft tube surging region, recording the frequency and amplitude of pressure fluctuations occurring in the draft tube at each test point. In addition to the test points in the surging region, the general operating characteristics of the model were recorded outside of the surging region to define the swirl parameter over the complete turbine hill curve.

Each run was made at a single wicket gate setting. The net head was maintained in the range of 110-130 ft for the majority of the tests; operation at desired points on the turbine hill curve was achieved by varying the runner speed. The operating status of the turbine model was recorded for each test point using the computerized data acquisition system. The flow in the draft tube throat section could be viewed with the aid of a strobe light. Photographs of the helical vortex were taken at many of the test points. The vortex was made visible either by cavitation occurring in the vortex core or by injection of air into the draft tube. These flow visualization techniques have been used by other investigators (Nishi et al., 1982).

To minimize the possible influence of two-phase flows, an effort was made to conduct all tests at the maximum tailwater level, dictated by the height of the downstream standpipe. This was intended to produce a non-cavitated vortex at all operating points. Operation under these conditions yielded a cavitation coefficient σ of about 0.38 to 0.42 for the majority of the tests. Tests by Allis-Chalmers (1976) indicated that efficiency loss due to cavitation begins as σ drops below about 0.1 to 0.15, depending on the gate opening and speed ratio. Mollenkopf and Raabe (1970) found that the amplitude and frequency of pressure pulsations due to draft tube surging are independent of the cavitation coefficient when operation is at a cavitation coefficient above that causing efficiency loss.

4.3 WICKET GATE SETTING

The wicket gate setting of the turbine is controlled by a manual hand wheel. A digital counter is used to determine the gate setting. The calibration data for the wicket gates was provided by USBR personnel who worked with the turbine model at Estes Power Plant (personal communication, Thomas Isbester, retired, USBR, Denver, Colorado). Additionally, an efficiency hill curve developed while the model was at Estes Power Plant was provided.

In the process of moving the model turbine to Colorado State, the handwheel and digital counter were removed from the turbine to avoid damage. After installation of the turbine, it was found that the gate calibration and efficiency hill curve developed at Estes Power Plant were no longer consistent. An analysis of the gate calibration was performed, and it was found that an error of 2.2° had been introduced into the calibration. The gate calibration provided by the USBR was adjusted by 2.2° and this calibration was used for the project. The gate calibration is given in Appendix C. The fully open gate setting for the prototype unit is 34° .

4.4 PRESSURE FLUCTUATION MEASUREMENTS

Pressure surges in the draft tube were measured using two piezoresistive pressure transducers mounted at the draft tube throat, just below the runner exit. The transducers were located 180° apart, on the upstream side of the draft tube (location T1) and on the tailrace side (location T2), as in Figure 4-1. Amplitude and frequency data were collected from transducer location T1, using a dynamic signal analyzer. A digitizing oscilloscope was used to simultaneously capture time domain signal traces from both transducers. Comparison of the phase relationships of the two signals was used as an indicator of synchronous or asynchronous surging. Calibrations of the transducers were determined before testing began and were rechecked after testing was completed. The calibration curves are included in Appendix C.

4.4.1 Frequency Spectra

The amplitude and frequency of pressure fluctuations at location T1 were recorded in the form of frequency spectra using a Hewlett Packard 3561A Dynamic Signal Analyzer. The AC coupling feature of the analyzer was used so that only the fluctuation of pressure would be recorded, rather than its absolute value. The

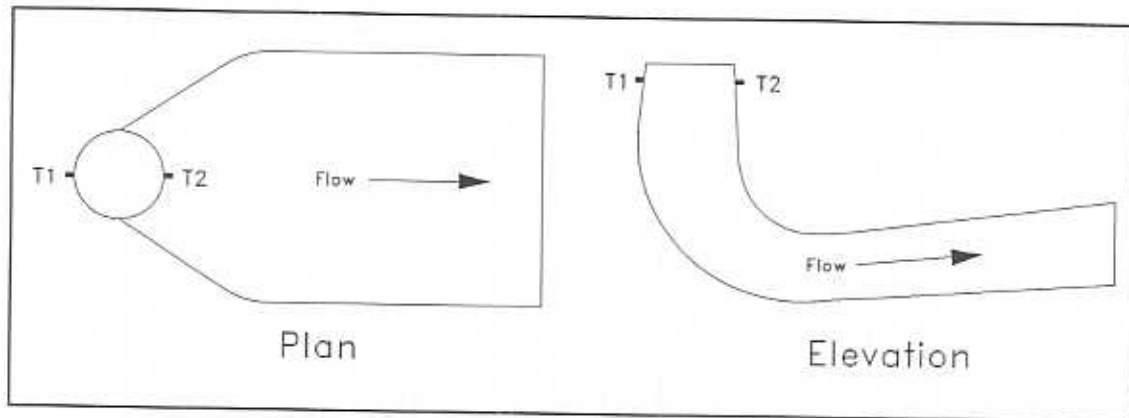


Figure 4-1. Schematic of pressure transducer locations.

selection of AC coupling places a capacitor in series with the input signal to remove the DC component. This works reliably for frequencies as low as 1 Hz. The data of interest for this project were at frequencies of about 7 Hz and higher.

Frequency spectra were collected for each operating point in the draft tube surging zone. The frequency range used for the measurements was 0-200 Hz. A flattop window function was used in all cases. This window function provides accurate amplitude measurements with reduced leakage. Each of the spectra recorded was taken using the RMS Averaging feature of the signal analyzer. Frequency spectra recorded during 10 consecutive sampling periods were averaged by the signal analyzer and the resulting average was output to the display of the analyzer. The RMS Averaging technique does not remove noise from the signal, but produces a more accurate estimate of the amplitude of the total signal plus noise.

Signal amplitudes were recorded in dBV by the signal analyzer. The peak amplitude and the frequency at which it occurred were automatically marked by the signal analyzer. Other significant frequencies and their amplitudes were recorded by hand on the spectrum plots.

4.4.2 Phase Relationships

To distinguish between synchronous and asynchronous surging conditions, information about the phase of pressure fluctuations at locations T1 and T2 was desired. A Hewlett Packard 54501A Digitizing Oscilloscope was used to record the signals from the T1 and T2 transducer locations simultaneously. The signals could be displayed side by side and a qualitative determination made as to whether the signals were in phase or out of phase.

4.5 PROBLEMS

The collection of pressure data was sometimes hampered by the unsteady flow of significant quantities of air through the turbine model. At points upstream of the model, there are locations where air pockets may collect in the pipeline. After several minutes of operation, the majority of this air is entrained into the flow and carried through the model. However, some pockets of air remain, and are then entrained into the flow when the discharge is varied. When these pockets of air pass through the draft tube a very large fluctuation in pressure is detected by the pressure transducers. Every effort was made to ensure that during the time data was being collected, the flow was free of these pockets of air. The usual effect of the air was to cause an overload to be indicated by the signal analyzer, after which the instrument was reset and the measurement repeated.

CHAPTER 5

ANALYSIS AND RESULTS

Data were collected at 108 operating points at 14 different wicket gate settings. Pressure fluctuation data were obtained for 74 points in the positive swirl, draft tube surging region. All of the collected data are included in Appendix A. In general, the dominant pressure fluctuation occurred at the precession frequency of the helical vortex, which was easily observed using a strobe light. Quantitative analysis was restricted to the dominant frequency, although some test points exhibited significant pressure fluctuations at higher harmonics of the dominant frequency.

5.1 REDUCTION OF THE DATA SET

Despite the use of the maximum available tailwater, the helical vortex was cavitated at many operating points. To evaluate the effect of the cavitated vortex, pressure fluctuation data were taken at several points under both high and low tailwater conditions. At low tailwater conditions the vortex was well cavitated at these points. At high tailwater levels, the vortex core was primarily filled with liquid water; just enough cavitation remained to make the vortex visible. The operation of the model was adjusted so that the operating point on the hill curve was approximately the same for both the high tailwater and low tailwater observations. Table 5-1 compares the pressure fluctuations at high and low tailwater levels. It was found that in the positive swirl region, the cavitated vortex had little effect on the amplitude or frequency of the pressure fluctuations. This is consistent with the observations of Mollenkopf and Raabe (1970) and Palde (1974). As a result, no distinction was made in further analysis between cavitated and non-cavitated vortex

conditions. However, since the cavitation coefficient is not accounted for in the dimensional analysis of the draft tube surge problem, the requirement that all tests be conducted at high tailwater levels (i.e., approximately the same cavitation coefficient) was retained. Thus, data collected at low tailwater levels were not included in the analysis. This eliminated nine test points from the data set.

Table 5-1. Effect of tailwater levels on pressure fluctuations.

Run	Wicket Gate Setting (degrees)	Swirl Parameter	σ	Dominant Frequency (Hz)	RMS Amplitude (psi)	Frequency Parameter	Pressure Parameter
3-8	30.2	0.43	0.369	12.5	1.03	0.48	0.18
3-9	30.2	0.42	0.247	12.5	0.92	0.47	0.16
4-7	26.2	0.67	0.430	11.5	2.03	0.52	0.50
4-8	26.2	0.64	0.294	11.5	2.12	0.52	0.51

In addition to the pressure fluctuations caused by the draft tube surge, several other sources of pressure fluctuations are present in the model turbine. These include the runner rotational frequency, bucket passing frequency, and wicket gate passing frequency. Only the runner rotational frequency occurs at frequencies low enough to be possibly confused with the draft tube surge. The runner rotational frequency was calculated for each test point and compared to the observed pressure fluctuation frequency spectrum. Many of the spectra show a significant pressure fluctuation at the runner rotational frequency; the runner rotational frequency was the dominant frequency at five of the test points. All pressure fluctuations at the runner rotational frequency were eliminated from the data set.

Two possible sources of hydraulic resonance were identified in the test stand. The penstock leading from the head tank to the model and the draft tube section from the runner exit to the tailwater tank are both susceptible to water hammer. The length of the penstock and spiral case was determined from engineering drawings of the test facility to be about 11 ft, along the conduit centerline. The

length of the draft tube was determined to be about 60 in. from the draft tube inlet to the connection point with the tailwater tank; a free surface was maintained in the tailwater tank for all tests. Assuming a wave celerity of 4000 ft/s, the natural frequencies of the penstock and draft tube were estimated to be 91 Hz and 200 Hz, respectively. This is well beyond the range of frequencies generated by the draft tube surge. Thus, resonance in the draft tube or penstock did not influence the measurements.

After reduction of the data set, pressure fluctuation data from 60 test points in the positive swirl, draft tube surging region were available for analysis. The data for these 60 test points are shown in Table A-1 in Appendix A.

5.2 GENERAL OBSERVATIONS

Figure 5-1 shows the efficiency hill curve for the model turbine, with test points marked on the plot. The operating range of the prototype unit is also indicated on the plot by the vertical lines at speed ratios of 0.88 (maximum head = 355 ft) and 1.12 (minimum head = 220 ft). Figure 5-2 shows the lines of constant swirl for the model, plotted on the same axes as the hill curve. A comparison of the two figures shows that the zero swirl line passes just to the left of the best efficiency point; there is a slight positive swirl when operating at best efficiency.

5.2.1 Onset of Surging

A comparison of Figures 5-1 and 5-2 shows that the boundary between surging and non-surging flow does not coincide with a single line of constant swirl over the full range of wicket gate settings. Figure 5-3 shows the minimum swirl parameter at which a helical vortex and associated pressure pulsations were observed for each gate setting. The critical swirl value increases dramatically at small wicket gate settings. Table 5-2 shows the data used to construct Figure 5-3.

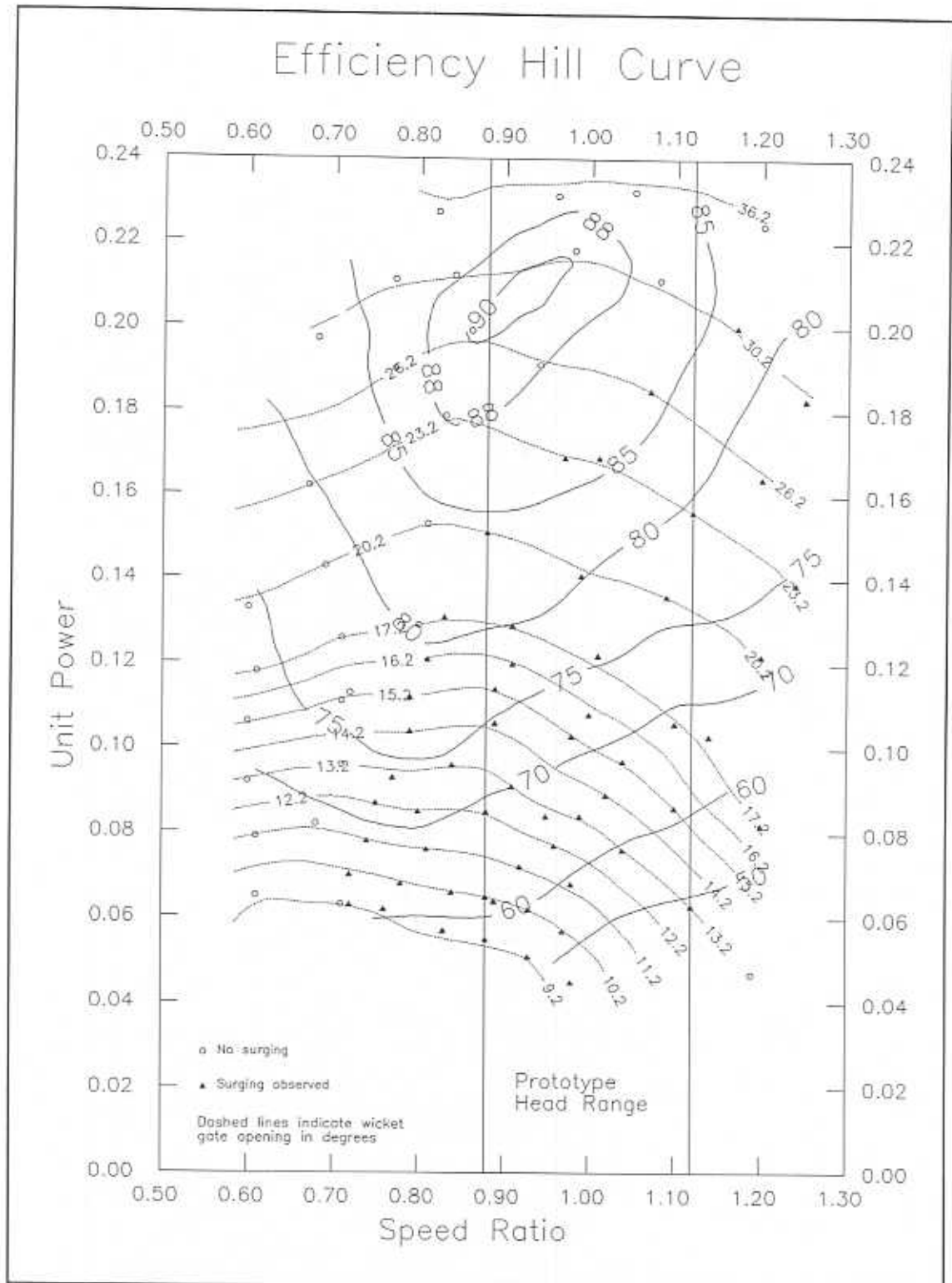


Figure 5-1. Efficiency hill curve and draft tube surging test points. Solid markers indicate test points at which significant pressure fluctuations were recorded. Solid lines are lines of constant efficiency (percent). Dotted lines are lines of constant wicket gate opening.

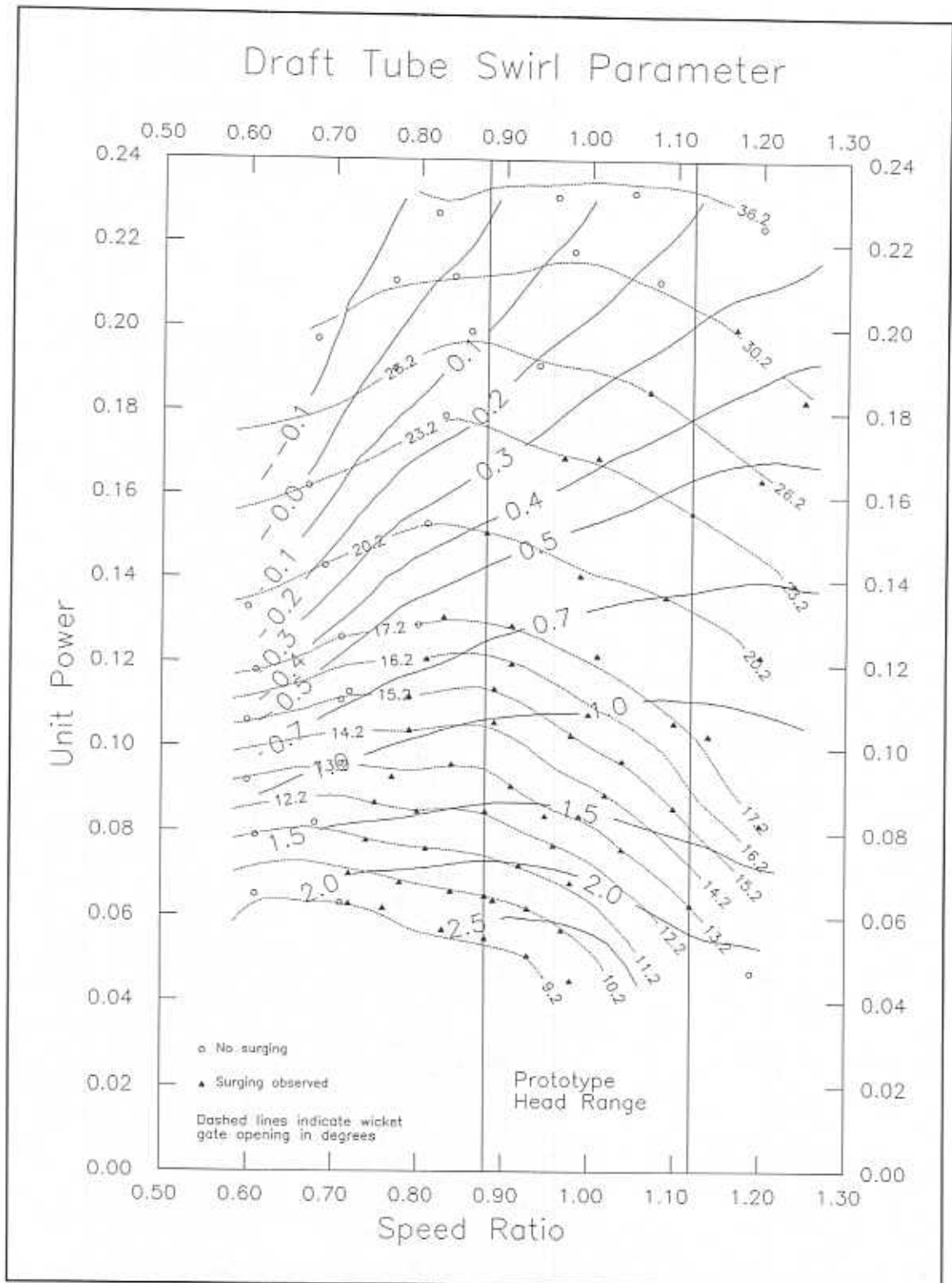


Figure 5-2. Draft tube swirl parameter map. Solid contours are lines of constant swirl parameter. Dotted lines indicate lines of constant wicket gate opening. Solid markers indicate test points at which significant pressure fluctuations were recorded.

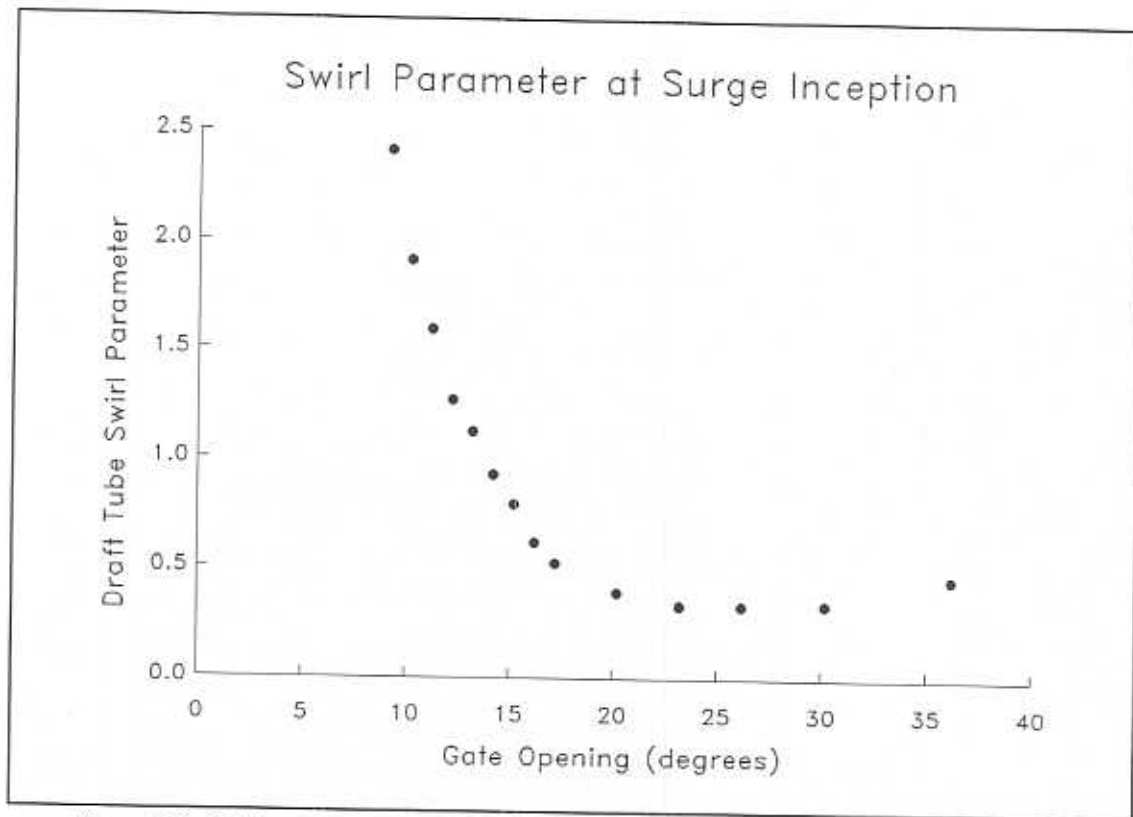


Figure 5-3. Swirl parameter at surge inception. The plot shows the minimum swirl value at which a helical vortex and associated pressure pulsations were observed for each wicket gate setting.

Table 5-2. Surge inception data.

Run	Gate Opening (degrees)	Swirl Parameter
10-3	9.2	2.41
13-1	10.2	1.91
11-3	11.2	1.59
14-1	12.2	1.27
12-3	13.2	1.13
15-1	14.2	0.93
8-4	15.2	0.79
17-1	16.2	0.62
7-4	17.2	0.53
6-4	20.2	0.39
5-3	23.2	0.33
4-5	26.2	0.33
3-7	30.2	0.34
2-8	36.2	0.46

In air model tests (no runner) of the elbow type draft tube for the turbine at Fontenelle Dam (Wyoming), Falvey and Cassidy (1970) found that surging occurred at swirl values above 0.4 (the Fontenelle and Grand Coulee draft tubes are similar,

though not identical, in shape). This is comparable to the critical swirl values observed in these tests at gate openings above about 20° . It should be noted that at gate settings of 20° - 28° the onset of surging occurs within the prototype operating range of the Grand Coulee Third Power Plant units; at larger or smaller gate openings, the onset of surging occurs outside of the prototype operating range (Figures 5-1 and 5-2). Thus, within the prototype operating range, the critical swirl identified in these tests agrees with that observed in the air model of the Fontenelle draft tube.

5.2.2 Vortex Breakdown

The development of the draft tube surge in the model followed the well known sequence described in the literature. At negative swirl values, a straight vortex was seen along the axis of the draft tube. As the swirl became less negative, the vortex decreased in diameter, finally vanishing, leaving the flow through the draft tube completely clear. In this region the swirl was approximately zero and the flow was approximately axial as it left the turbine runner. There were no significant pressure pulsations.

As the swirl was increased from this point, the flow remained clear until a critical point at which vortex breakdown occurred suddenly, and a helical vortex developed in the draft tube in the form of a left handed screw. The vortex precession was in the same direction as the runner rotation. The precession frequency of the vortex was about one-third to one-fourth of the rotational frequency of the runner. Pressure fluctuations in the draft tube occurring at the precession frequency were asynchronous; the signals from locations T1 and T2 were approximately 180° out of phase with one another, as shown in Figure 5-4.

At gate settings of 19.2° to 36.2° the pressure fluctuations and the size of the helical vortex core tended to increase with increasing swirl. Also, the pitch of the

helical vortex tended to increase as the swirl increased (i.e., the vortex became stretched out along the draft tube axis). However, the basic character of the flow remained unchanged.

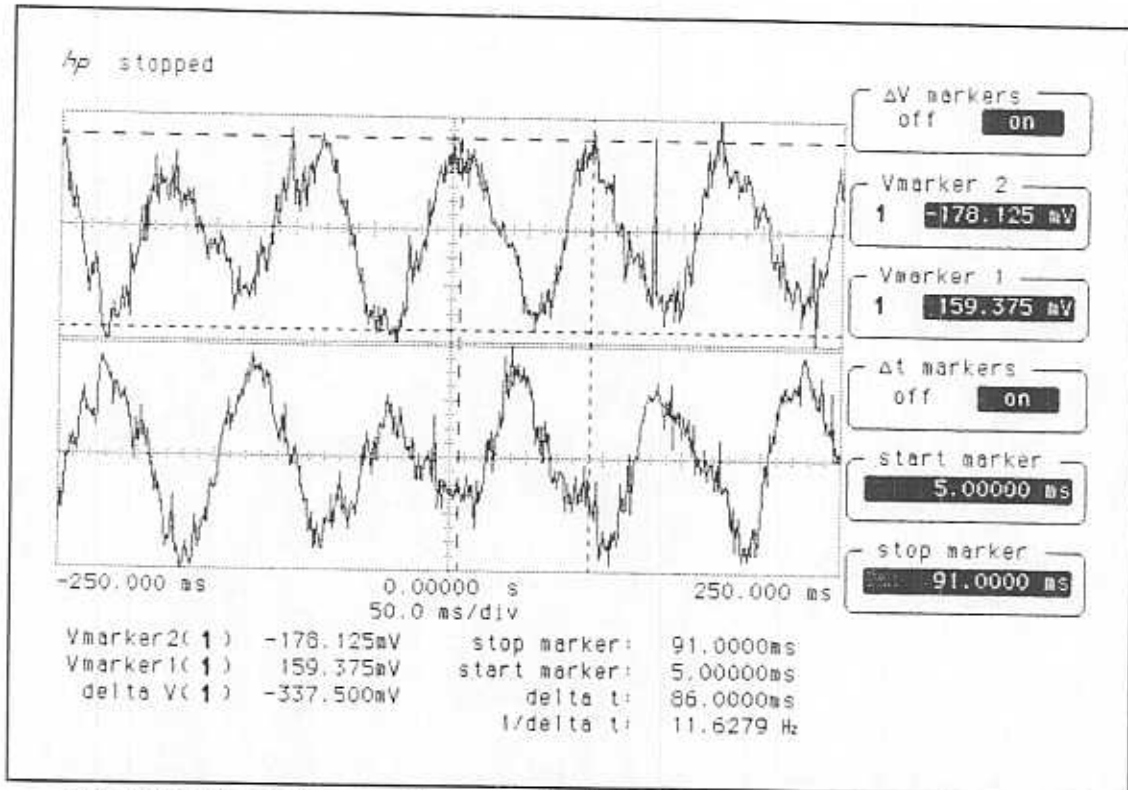


Figure 5-4. Phase of pressure fluctuations in single vortex region. The top signal is from T1; the bottom signal is from T2. This signal was recorded on Run 5-9.

5.2.3 Twin Vortex

As the swirl was increased at gate settings of 17.2° or lower, the vortex became less cavitated, until it was no longer easily visible at high tailwater levels. The vortex could be seen only at low tailwater levels; injection of air into the draft tube at high tailwater produced only a cloud of widely dispersed bubbles in the flow. Despite the disappearance of the vortex, pressure fluctuations were still detected in the draft tube at frequencies corresponding to the precession of a single helical vortex.

When the swirl was increased further still, the dominant frequency of pressure pulsations began to shift randomly between two different frequencies. The lower frequency corresponded to the precession of the single helical vortex. The higher

frequency was generally more than twice the lower frequency. Air injected into the draft tube continued to produce only a cloud of bubbles. As the swirl was increased past this point, the dominant frequency shifted completely to the higher frequency. When the tailwater was then lowered, two helical vortices could be seen in the draft tube, as in Figure 5-5. The vortex precession frequency, determined by observation using the strobe light, was one-half the dominant frequency of the pressure fluctuations. Each vortex retained the left handed orientation of the original single vortex. Simultaneous with the formation of the twin vortex, the signals at locations T1 and T2 became in phase with one another, as in Figure 5-6.



Figure 5-5. Photograph of twin vortex. The vortices were made visible by lowering the tailwater until the cores became cavitating. The photo was taken by matching the exposure setting of the camera to the strobe light frequency. The photo is from Run 8-8.

At the 17.2° gate setting, only the random shifting of the dominant frequency could be seen on the signal analyzer; attempts to get an RMS averaged frequency spectrum for either the single or twin vortex were unsuccessful. However, at gate settings of 16.2° and below, the twin vortex behavior became well established and frequency spectra were obtained.

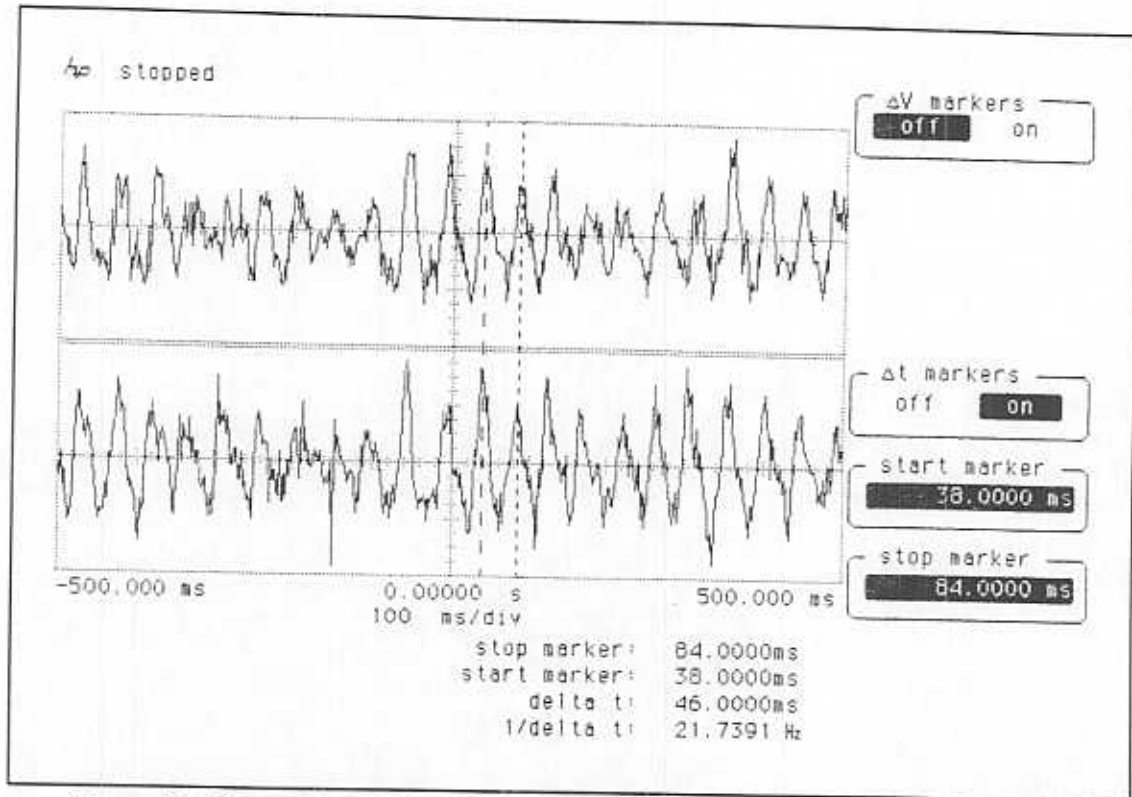


Figure 5-6. Phase of pressure fluctuations in twin vortex region. The top signal is from T1, while the bottom is from T2. This signal was recorded on Run 8-8.

At one test point at the 10.2° gate setting, both single and twin vortex modes persisted long enough that frequency spectra could be obtained for each mode. Figure 5-7 shows these frequency spectra. The spectrum with the maximum amplitude at 8 Hz corresponds to the single vortex; signals from T1 and T2 were 180° out of phase at the time. The spectrum with peak amplitude at 20 Hz was taken while signals from T1 and T2 were in phase, and corresponds to the twin vortex.

This behavior is similar to that noted by Fisher, Ulith, and Palde (1980) in their review of hydraulic model and prototype tests done on the Grand Coulee Third, Marimbondo, and Cerron Grande turbines. These three installations used nearly homologous turbines and similar elbow type draft tubes. In tests conducted by Allis-Chalmers on a 1:28 scale model of the Grand Coulee Third turbines, an oscillation between two different dominant frequencies was observed at about 46

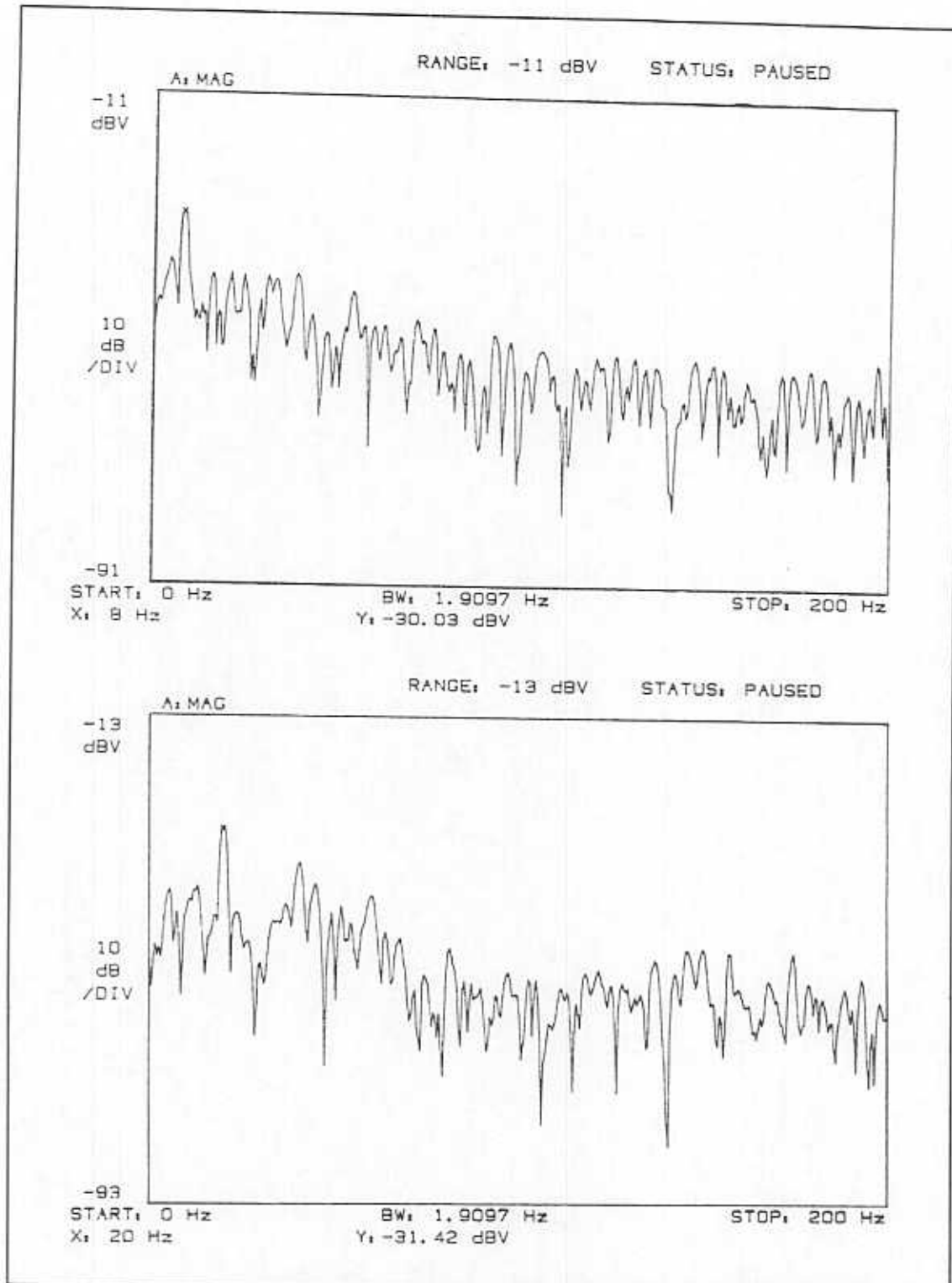


Figure 5-7. Comparison of single and twin vortex frequency spectra. These spectra were both recorded on Run 13-5. The top plot corresponds to the single vortex mode. The peak amplitude at 8 Hz matches the precession frequency of the single vortex. The lower plot corresponds to the twin vortex mode. The precession frequency of the twin vortices was observed to be 10 Hz using a strobe light; the dominant frequency of pressure pulsations is 20 Hz.

percent of the best efficiency gate setting. This corresponds to about a 12° gate setting. This behavior was also observed in model tests for the Marimbondo turbines at approximately the same gate setting. The vortex was apparently not visible in either test.

5.2.4 Higher Frequency Surge

As the swirl was increased further at low gate openings, the twin vortex appeared to break down. The dominant frequency increased as the swirl increased, and it was no longer possible to make the vortex visible by either cavitation or air injection. Near the limit of the operational range of the model, the dominant frequency was approximately equal to the runner rotational frequency. At this point it was difficult to conclude that the pressure fluctuations were related to the flow in the draft tube; they may have been due simply to the rotation of the runner. The region between the twin vortex and the point where the rotational frequency becomes dominant is referred to as Region III on the figures that follow in this chapter.

5.3 FREQUENCY PARAMETER

The frequency parameters for the dominant pressure fluctuation observed at each operating point were plotted on the same axes as the hill curve, and lines of constant frequency parameter were constructed. Figure 5-8 shows the frequency parameter contour map. The twin vortex region appears on this plot as a bench. The figure indicates a gradual increase in the frequency parameter leading into the twin vortex region. This is the result of smoothing performed in the conversion of the data to a grid suitable for plotting; experimental observations indicated that the increase in the frequency parameter due to the twin vortex was actually quite sudden.

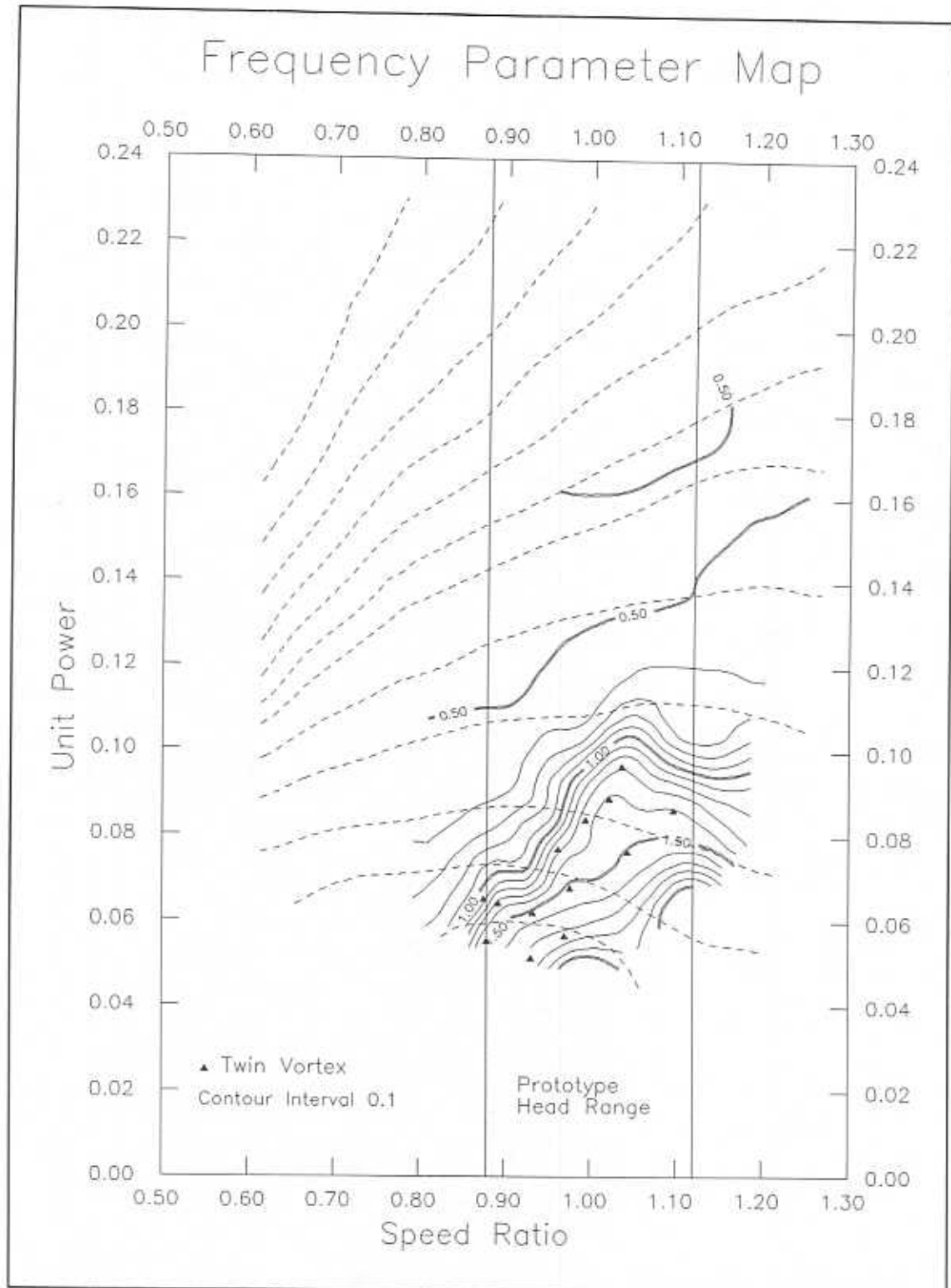


Figure 5-8. Frequency parameter map. Marked points indicate test points where a twin vortex was observed. Solid contours are lines of constant frequency parameter. Dashed lines are contours of the draft tube swirl parameter (from Figure 5-2).

Figure 5-9 shows the relationship of the dominant frequency parameter to the swirl parameter. The figure shows that a definite relationship exists between the frequency and swirl parameters. It should be emphasized that this particular relationship holds only for this specific draft tube shape. The figure clearly differentiates between the single and twin vortex. At swirl values less than about 1.2, only the single vortex mode occurs. However, as the swirl increases above 1.2, the possibility exists that the draft tube surge may consist of either a single or twin vortex. At these swirl values, the frequency parameter is no longer a single valued function of the swirl. The only way to predict the presence of the single or twin vortex is to refer to the frequency parameter map in Figure 5-8.

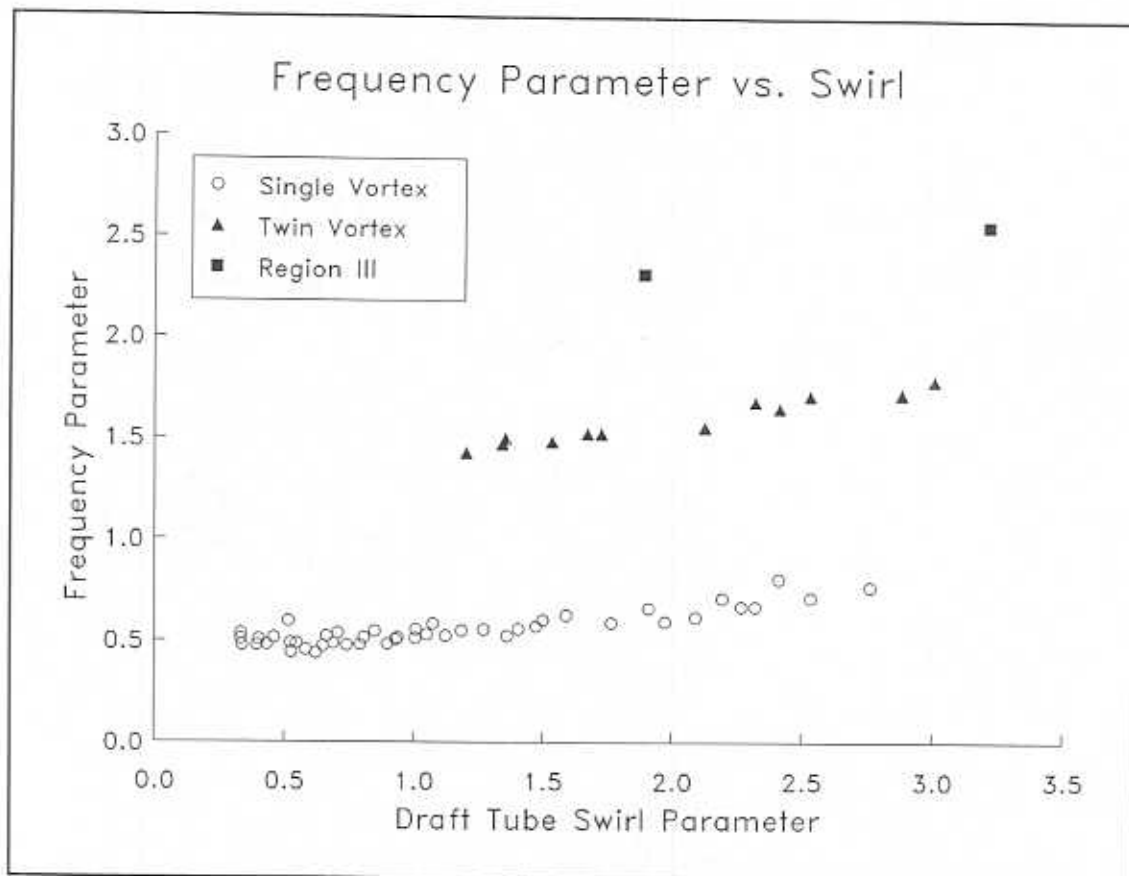


Figure 5-9. Frequency parameter vs. draft tube swirl parameter.

5.4 PRESSURE PARAMETER

A map of the pressure parameters corresponding to the dominant pressure fluctuation at each test point was constructed. Figure 5-10 shows two peaks in the pressure parameter, separated by a low saddle. The saddle region corresponds roughly with the region in which the twin vortex was observed. Comparison of this figure with the swirl parameter map (Figure 5-2) reveals that at low gate settings the pressure parameter contours bear little relationship to the swirl contours. To better illustrate this fact, the pressure parameter values were plotted against the swirl parameter in Figure 5-11. Points where a twin vortex was observed are marked on the plot.

Figure 5-12 shows the same data divided between small gate openings (9.2° - 16.2°) and large gate openings (17.2° - 36.2°). The pressure parameter correlates well with the swirl parameter at the large gate settings. However, in the lower range of gate settings, the pressure parameter varies widely. As with the frequency parameter, variation of the pressure parameter is better explained by the pressure parameter map (Figure 5-10).

5.5 HARMONICS

Several test points exhibited significant pressure fluctuations occurring at second or higher harmonics of the vortex precession frequency. These signals may arise from several different sources. For test points where a twin vortex was observed, the second harmonic of the vortex precession frequency was the dominant frequency of the pressure fluctuation, due to the fact that two vortices passed each transducer location during one precession period.

In the single vortex region, the dominant pressure fluctuation occurred at the vortex precession frequency, with the amplitude of higher harmonic frequencies generally decreasing as the number of the harmonic increased. This type of

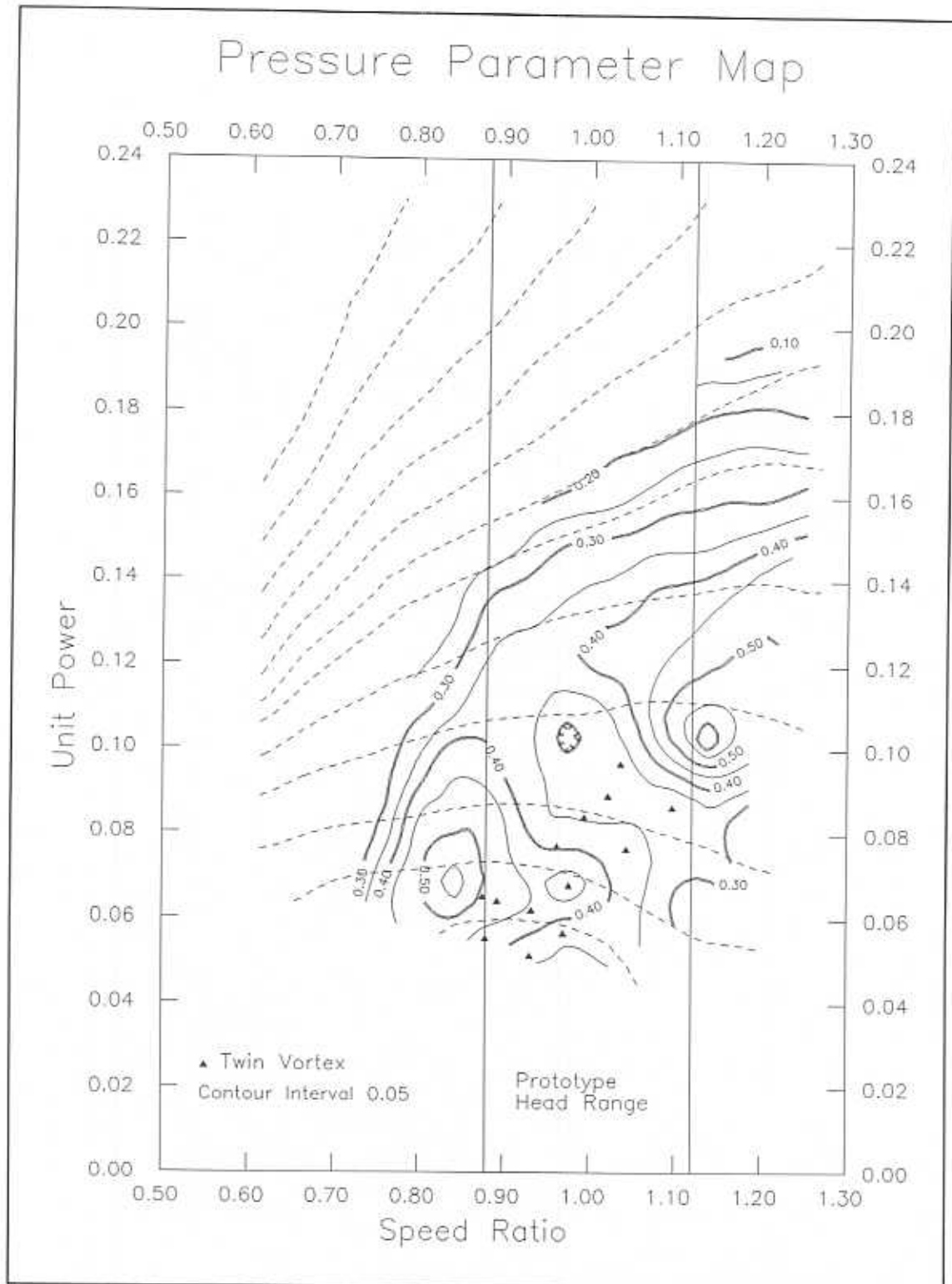


Figure 5-10. Pressure parameter map. Marked points indicate test points where a twin vortex was observed. Solid contours are lines of constant pressure parameter. Dashed lines are contours of the draft tube swirl parameter (from Figure 5-2).

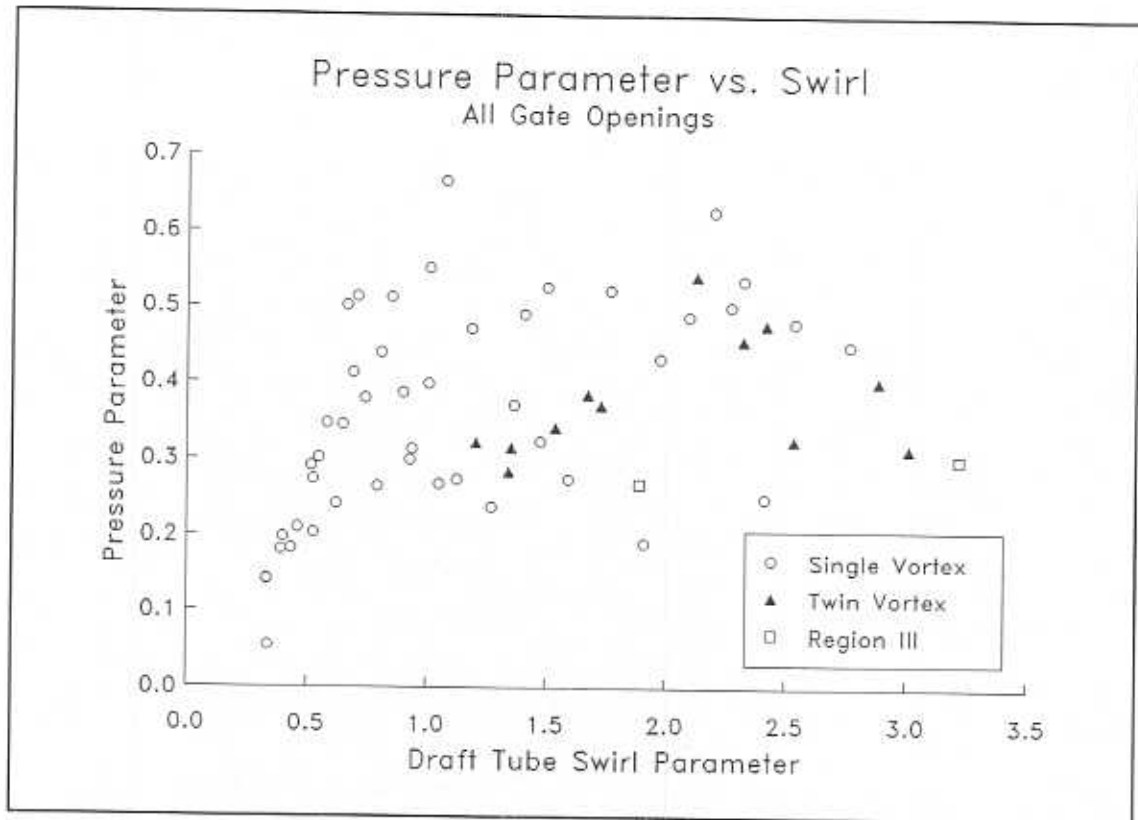


Figure 5-11. Pressure parameter vs. swirl for all gate settings.

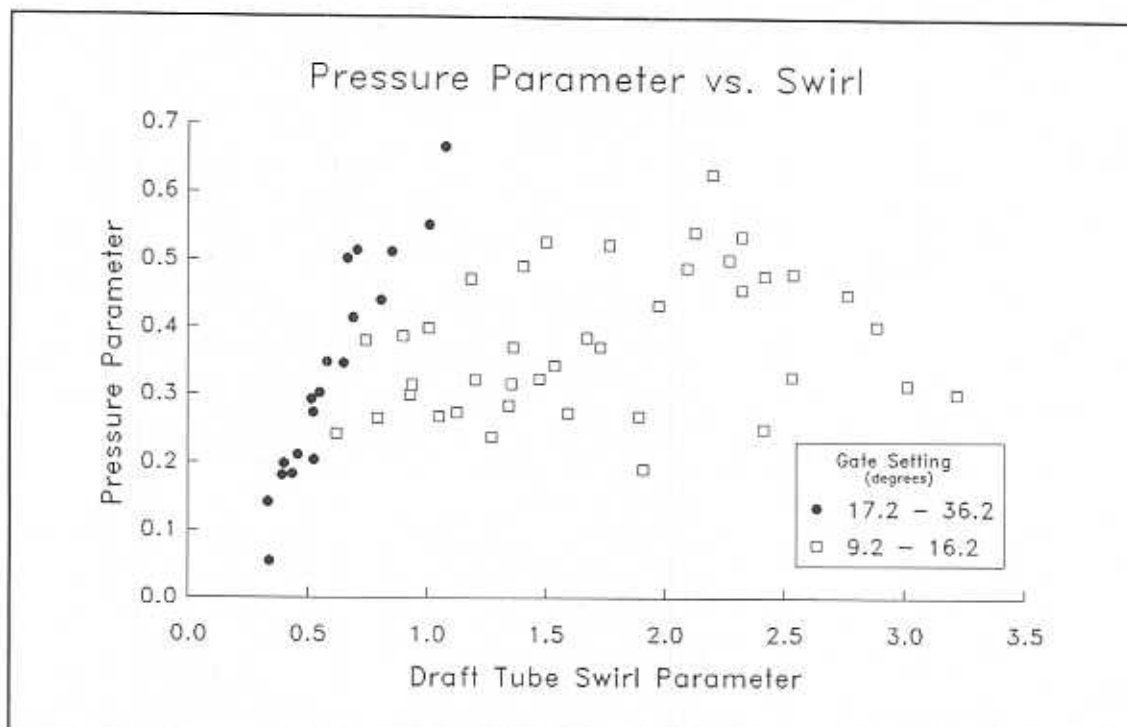


Figure 5-12. Pressure parameter vs. swirl by gate setting.

frequency spectrum often indicates that the waveform is distorted from a sinusoidal shape. Many of the time domain traces show signals having sharp peaks, somewhat like a saw-tooth wave. Figure 5-13 shows one non-sinusoidal signal and the resulting frequency spectrum. Fanelli (1989) suggests that a cavitated vortex core is most likely to produce these types of distorted signals.

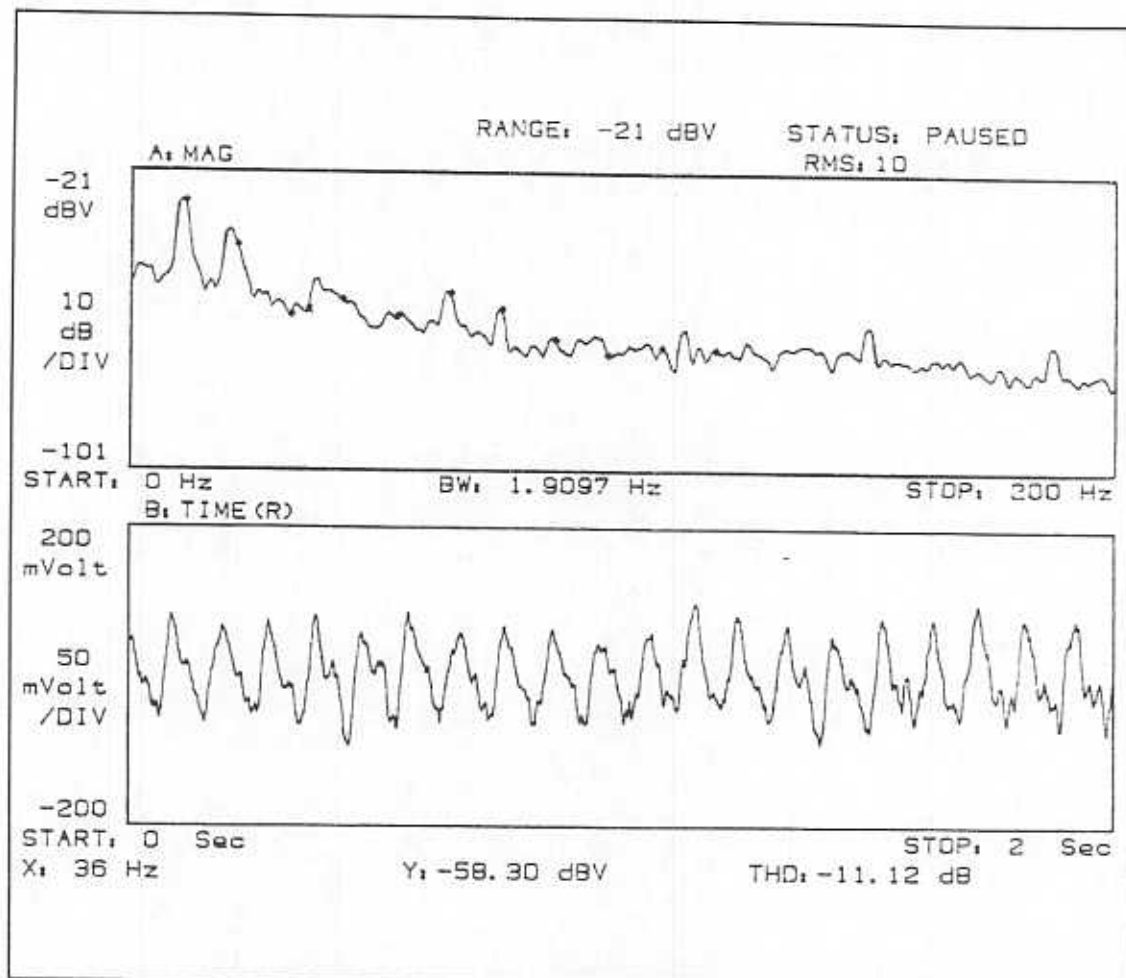


Figure 5-13. Effect of non-sinusoidal pressure fluctuations. The dominant frequency is 10.5 Hz, with an amplitude of -29.00 dBV. The second peak is at 20.0 Hz, with an amplitude of -36.95 dBV. This frequency spectrum was recorded on Run 5-4; the vortex was cavitating.

5.6 SYNCHRONOUS AND ASYNCHRONOUS SURGING

The placement of the T1 and T2 transducers directly opposite one another in the draft tube was intended to indicate the presence of synchronous or asynchronous pressure fluctuations. Synchronous surging would cause pressure fluctuations involving the entire draft tube, so that the two transducers would be in phase. Asynchronous surging would produce signals associated with the precession of the helical vortex; the signals would be 180° out of phase.

In the twin vortex region, the signals at T1 and T2 were always in phase with one another. Despite this, it can not be concluded that the twin vortex is a synchronous surge. A synchronous surge produces pressure fluctuations that are in phase with one another throughout the draft tube. The fact that T1 and T2 are in phase can be easily accounted for by the presence of two asynchronous pulsations, associated with each of the two vortices, located 180° opposite one another. In order to determine if synchronous surging exists in the twin vortex zone, an additional transducer location would be required.

Synchronous surging with both transducers in phase could not be detected at any point in the single vortex surging region. However, at several test points there were indications that the surge contained a synchronous component. In several of the time domain traces captured by the oscilloscope, the amplitudes of the pressure fluctuations were obviously different at the two transducer locations. Figure 5-14 shows one such trace. The signal at location T1 (top) is of significantly lower amplitude than the signal at location T2. The two transducers have nearly identical calibrations. This type of behavior was noted at 10 test points. The differences in amplitude were not evaluated quantitatively.

The differences in amplitude can be explained by the superposition of a synchronous pressure fluctuation that is in phase with the asynchronous fluctuation at T2 and out of phase with the asynchronous fluctuation at T1. The most interesting

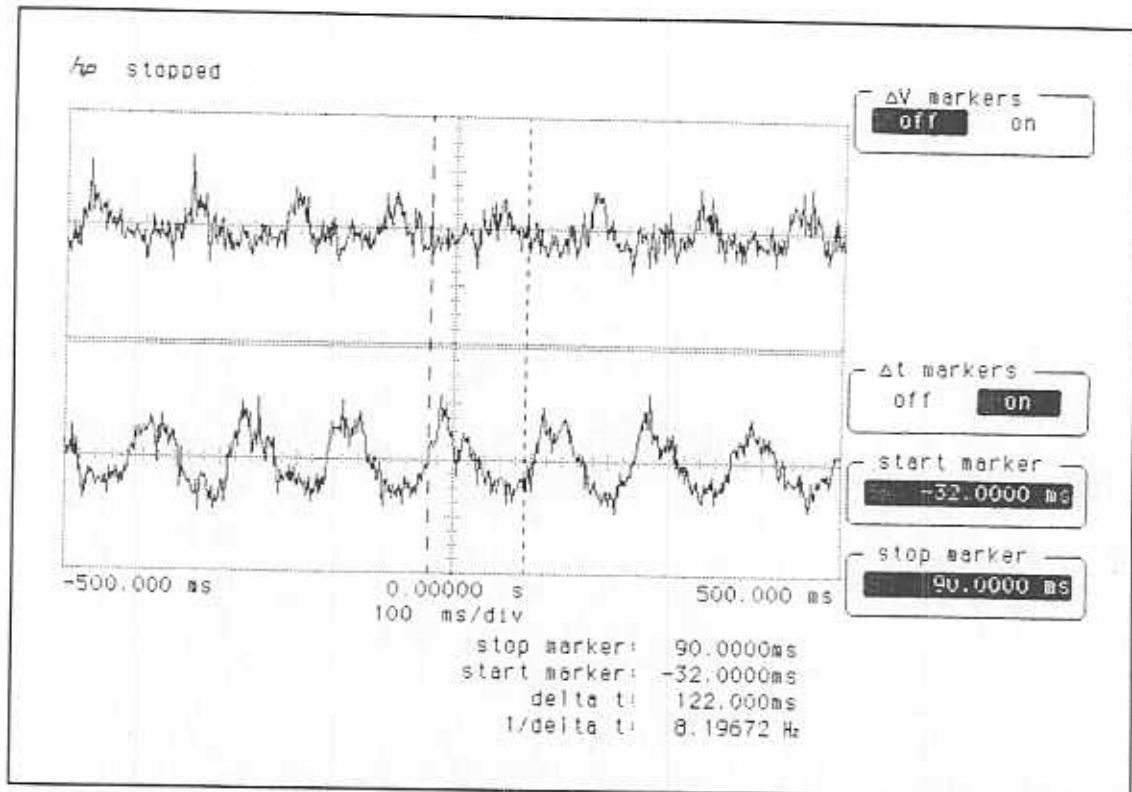


Figure 5-14. Differences in pressure pulsation amplitude. The top signal is from transducer location T1. The bottom signal is from location T2. These signals were recorded on Run 9-4.

aspect of the observations is that at each of the 10 points, the phase difference between the two signals remained about 180° , and the amplitude at T2 was always higher than that at T1. This implies that the phase relationship between the synchronous and asynchronous components is consistently the same, even for different operating points on the turbine hill curve. Also, the synchronous component must have a lower amplitude than the asynchronous component at each of these points.

The test points exhibiting this behavior are indicated on the pressure parameter map shown in Figure 5-15. Each of these test points is also indicated in Table A-2, Appendix A. The location of these points does not appear to be related to the twin vortex region; in fact, this behavior was not observed at any of the twin vortex test points.

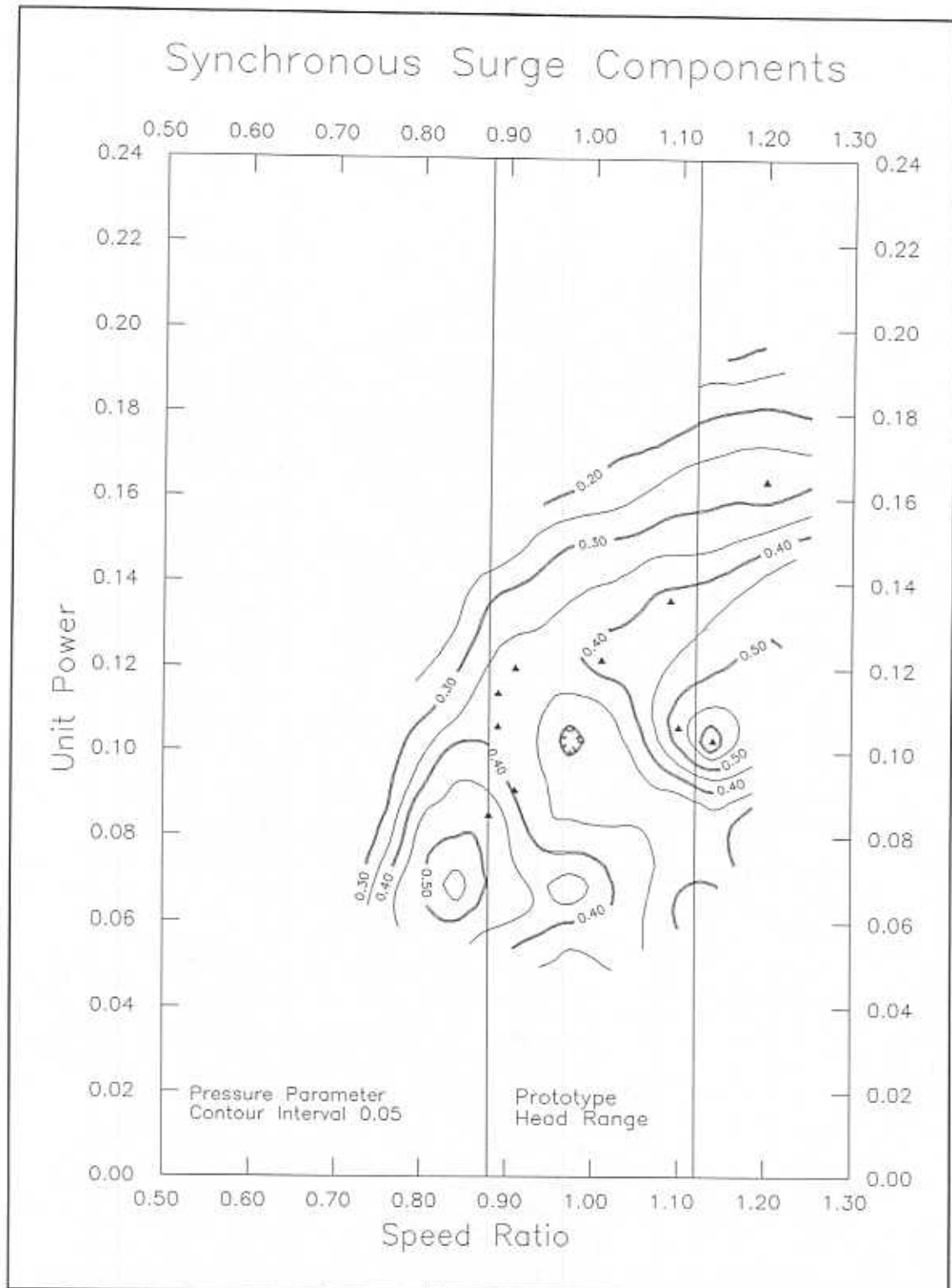


Figure 5-15. Test points with evidence of synchronous surging. At each of the indicated points, the amplitude of the pressure fluctuation at T2 was significantly higher than the amplitude at T1, as seen on the oscilloscope trace. Solid contours are lines of constant pressure parameter.

CHAPTER 6

CONCLUSIONS AND RECOMMENDATIONS

6.1 CONCLUSIONS

On the basis of dimensional analysis and prior research, the hypothesis was made that for a given draft tube shape, operating at a high Reynolds number, the amplitude and frequency of draft tube surge pressure pulsations is dependent only on the value of the draft tube swirl parameter. However, these model tests indicate that the draft tube swirl parameter does not fully explain the behavior of the draft tube surge over the complete operating range of the model turbine. Specifically, the following conclusions can be drawn from this study:

- * The pressure parameter is related to the swirl parameter only at high wicket gate settings (above about one-half of the full gate opening). At low gate settings, there is little relationship between the pressure parameter and the swirl parameter; variation of the pressure parameter was better explained by the pressure parameter map.
- * The frequency parameter is dependent not only on the value of the draft tube swirl parameter, but also on the number of helical vortices in the draft tube. At swirl values above 1.2, the frequency parameter becomes a multi-valued function of the swirl, depending on whether the flow contains a single or twin vortex. Again, location of the test point on the turbine hill curve and reference to the frequency parameter map is necessary for predicting the value of the frequency parameter.

- * The transition from the single to the twin vortex is unstable. In the transition zone, either form may exist, and the flow in the draft tube seems to alternate randomly between the two modes.
- * In the region of the hill curve to the right and below the twin vortex region (i.e., higher swirl), the frequency parameter increases further, with the frequency of pressure pulsations approaching the rotational frequency of the runner. This behavior also can not be discerned from calculation of the swirl parameter alone; one must refer to the frequency parameter map.
- * The critical swirl value corresponding to the onset of surging varies with the wicket gate setting. At wicket gate settings above about 20° , the critical swirl value varies only slightly, and corresponds to that observed in air model tests of a similar elbow type draft tube. However, at lower gate openings, the critical swirl value increases rapidly as the gate opening decreases.
- * Several indicators of the twin vortex were identified. Some of these are applicable to field situations where the flow in the draft tube can not be observed visually. The indicators were:
 - a) visual observation of two vortex ropes
 - b) shift of the dominant pressure pulsation frequency from that generally associated with a single vortex, to a frequency about two and one-half times as high
 - c) pressure pulsations in phase on opposite sides of the draft tube
 - d) transition region in which both the single and twin vortex may exist alternately
 - e) reduction of the pressure parameter in and around the twin vortex region
- * The twin vortex is important as it is an excitation source at a frequency well above the Rheingans frequency generally associated with draft tube surging. If power plant components are designed with natural frequencies close to the

frequency associated with the twin vortex, then resonance problems may develop. If problems do occur, operation in the twin vortex region can not be avoided entirely. The pressure and frequency parameter maps show that the twin vortex exists over the full head range for the Grand Coulee Third prototype. Thus, the turbine will always be required to pass through the twin vortex region during startup and shutdown.

- * Evidence of synchronous components of pressure fluctuation were detected at several operating points. Although the synchronous pulsations were not evaluated quantitatively, it was observed that the synchronous component, when present, had a consistent phase relationship with the asynchronous component, independent of the operating point of the turbine. In addition, the synchronous component was always lower in amplitude than the asynchronous component. The location of these test points was not related to the twin vortex region.

6.2 RECOMMENDATIONS FOR FURTHER RESEARCH

Synchronous pressure pulsations are accepted as the driving mechanism behind most operational problems related to draft tube surging, although in some cases simple vibration and noise caused by asynchronous pulsations can be serious. Synchronous pressure fluctuations can produce variations in head, discharge, torque, and output power. Unfortunately, measurements of pressure pulsations have generally been made at single points on the draft tube wall, rather than measuring the pulsations of average pressure at a given cross section.

Piezometer manifolds are often used to obtain the average pressure at a given cross section in hydraulic studies. However, in the case of the rotating pressure field due to the helical vortex, the use of a manifold with multiple taps into the tube would produce false pulsations in the manifold at the tap passing frequency for the helical vortex.

A better approach would be to employ a multi-channel analyzer capable of measuring both the phases and amplitudes of pressure fluctuations at three or more individual taps located around the draft tube. The phases and amplitudes at a given frequency from each location, plotted in the complex plane, should define a circle. The displacement of the circle from the origin would be the amplitude of the synchronous component, while the radius of the circle would be the amplitude of the asynchronous component.

The existence of a twin vortex surging mode in this hydraulic model has been confirmed, and evidence in the literature suggests that other, nearly homologous models also exhibit a twin vortex surge. Confirmation of the twin vortex in the Grand Coulee Third Power Plant prototype units would be a useful extension of this study. The Grand Coulee draft tubes are equipped with two mandrels located 180° opposite one another; a transducer arrangement similar to that employed on this model could be used.

It is possible that the twin vortex is unique to this particular turbine and draft tube combination and other nearly homologous units. Investigation of other non-homologous models and prototypes should be conducted.

Although the twin vortex was observed and the region of its occurrence was defined on the turbine hill curve, the cause of the transition from a single vortex to a twin vortex could not be identified. Identification of this cause should be a goal of further research.

It was noted during these tests that upon transition to the twin vortex surging mode, the dominant frequency of pressure pulsations increased by a factor significantly greater than two. Not only did the number of vortices double, but the precession frequency of the vortices also seemed to increase. Further investigation of this phenomenon should be conducted.

Investigations similar to those conducted for this project should be made for surging in the overload region (i.e., negative swirl). Observations by the author and others in field situations suggest that the surge behavior in the overload region is significantly different from that in the part-load region.

REFERENCES

- Allis-Chalmers Hydro-Turbine Division, "Grand Coulee Third Power Plant, Units No. 22, 23, and 24, Model Test Report," U. S. Bureau of Reclamation, Denver, Colorado, Customer Contract No. DS-7001, March 1976.
- Benjamin, T. B., "Theory of the Vortex Breakdown Phenomenon," *Journal of Fluid Mechanics*, Vol. 14, 1962, pp. 593-629.
- Benjamin, T. B., "Significance of the Vortex Breakdown Phenomenon," *Transactions of the ASME, Journal of Basic Engineering*, June 1965, pp. 518-524.
- Benjamin, T. B., and M. J. Lighthill, "On Cnoidal Waves and Bores," *Proceedings of the Royal Society of London, Series A*, Vol. 224, July 1954, pp. 448-460.
- Bhan, S., J. B. Codrington, and H. Mielke, "Reduction of Francis Turbine Draft Tube Surges," *Proceedings, Fifth International Symposium on Hydro Power Fluid Machinery*, Chicago, Illinois, 1988, pp. 95-102.
- Brigham, E. O., *The Fast Fourier Transform*, Prentice-Hall, Inc., Englewood Cliffs, NJ, 1974, 252 pp.
- Cassidy, J. J., "Experimental Study and Analysis of Draft Tube Surging," *REC-OCE-69-5, Report No. Hyd-591*, U. S. Bureau of Reclamation, Oct. 1969.
- Cassidy, J. J., and H. T. Falvey, "Observations of Unsteady Flow Arising After Vortex Breakdown," *Journal of Fluid Mechanics*, Vol. 41, 1970, pp. 727-736.
- Chanaud, R. C., "Observations of Oscillatory Motion in Certain Swirling Flows," *Journal of Fluid Mechanics*, Vol. 21, 1965, pp. 111-127.
- Dériaz, P., "A Contribution to the Understanding of Flow in Draft Tubes of Francis Turbines," International Association for Hydraulic Research, Hydraulic Machinery and Equipment Symposium, Nice, France, Sept. 1960.
- Escudier, M. P., and N. Zehnder, "Vortex Flow Regimes," *Journal of Fluid Mechanics*, Vol. 115, 1982, pp. 105-121.
- Falvey, H. T., "Draft Tube Surges - A Review of Present Knowledge and an Annotated Bibliography," *Report No. REC-ERC-71-42*, U. S. Bureau of Reclamation, Dec. 1971.

- Falvey, H. T., "The Anatomy of a Steady Oscillatory Flow Problem," *Proceedings, Fourth Meeting of the IAHR/AIRH Work Group on the Behaviour of Hydraulic Machinery under Steady Oscillatory Conditions*, Fort Collins, Colorado, Aug. 1989.
- Falvey, H. T., and J. J. Cassidy, "Frequency and Amplitude of Pressure Surges Generated by Swirling Flow," *Proceedings, 5th Symposium of the International Association for Hydraulic Research Section for Hydraulic Machinery Equipment and Cavitation*, Paper E1, Stockholm, Sweden, 1970.
- Fanelli, M., "The Vortex Rope in the Draft Tube of Francis Turbines Operating at Partial Load: A Proposal for a Mathematical Model," *Proceedings, Fourth Meeting of the IAHR/AIRH Work Group on the Behaviour of Hydraulic Machinery Under Steady Oscillatory Conditions*, Fort Collins, Colorado, Aug. 1989.
- Fisher, R. K., Jr., U. J. Palde, and P. Ulith, "Comparison of Draft Tube Surging of Homologous Scale Models and Prototype Francis Turbines," *Proceedings, 10th Symposium of the International Association for Hydraulic Research Section for Hydraulic Machinery Equipment and Cavitation*, Tokyo, Japan, 1980.
- Gearhart, W. S., A. M. Yocum, and T. A. Seybert, "Studies of a Method to Prevent Draft Tube Surge and the Analysis of Wicket Gate Flow and Forces," *Report No. REC-ERC-78-12*, U. S. Bureau of Reclamation, Apr. 1979.
- Grein, H., "Vibration Phenomena in Francis Turbines: Their Causes and Prevention," *Proceedings, 10th Symposium of the International Association for Hydraulic Research Section for Hydraulic Machinery Equipment and Cavitation*, Tokyo, Japan, 1980.
- Guarga, R., G. Hiriart, and J. J. Torres, "Oscillatory Problems at Mexico's La Angostura Plant," *Water Power & Dam Construction*, Oct. 1983, pp. 33-36.
- Harvey, J. K., "Some Observations of the Vortex Breakdown Phenomenon," *Journal of Fluid Mechanics*, Vol. 14, 1962, pp. 585-592.
- Heigel, L., A. B. Lewey, and J. P. Favero, "Turbine Performance Test - Unit G24, Grand Coulee Dam, Grand Coulee Third Powerplant, Columbia Basin Project," *Report Number HM-25*, U. S. Bureau of Reclamation, Dec. 1984.
- Hosoi, Y., "Experimental Investigations of Pressure Surge in Draft Tubes of Francis Water Turbines," *Hitachi Review*, Vol. 14, No. 12, 1965, pp. 2-12.
- Hosoi, Y., "Contributions to Model Tests of Draft Tube Surges of Francis Turbines," *Proceedings, Joint Symposium on Design and Operation of Fluid Machinery*, Fort Collins, Colorado, June 1978, pp. 141-150.
- Kito, F., "The Vibration of Penstocks," *Water Power*, Vol. 11, Oct. 1959, pp. 379-392.

- Koning, H. B., and W. G. Whippen, "Vibration Problems at Conowingo," *Water Power*, July 1967, pp. 259-260.
- Lecher, W., and K. Baumann, "Francis Turbines at Part-Load with High Back-Pressure," *Proceedings*, 4th Symposium of the International Association for Hydraulic Research Section for Hydraulic Machinery Equipment and Cavitation, Paper B4, Lausanne, Switzerland, 1968.
- Leibovich, S., "Vortex Stability and Breakdown: Survey and Extension," *AIAA Journal*, Vol. 22, No. 9, Sept. 1984, pp. 1192-1206.
- Mollenkopf, G., and J. Raabe, "Measurements of Fluctuations of Velocity and Pressure in the Draft Tube of a Francis Turbine," *Proceedings*, 5th Symposium of the International Association for Hydraulic Research Section for Hydraulic Machinery Equipment and Cavitation, Paper B3, Stockholm, Sweden, 1970.
- Nishi, M., T. Kubota, S. Matsunaga, and Y. Senoo, "Study on Swirl Flow and Surge in an Elbow Type Draft Tube," *Proceedings*, 10th Symposium of the International Association for Hydraulic Research Section for Hydraulic Machinery Equipment and Cavitation, Tokyo, Japan, 1980.
- Nishi, M., S. Matsunaga, T. Kubota, and Y. Senoo, "Flow Regimes in an Elbow Type Draft Tube," *Proceedings*, 11th Symposium of the International Association for Hydraulic Research Section for Hydraulic Machinery Equipment and Cavitation, Amsterdam, the Netherlands, 1982.
- Nystrom, J. B., "Effects of Tailrace Geometry on Draft-Tube Surging," Alden Research Laboratory, Worcester Polytechnic Institute, February, 1982.
- Nystrom, J. B., and P. M. Bozoian, "Effect of Tailrace Geometry on Draft Tube Surging," *Waterpower '83*, Proceedings of the International Conference on Hydropower, Knoxville, Tennessee, 1983.
- Palde, U. J., "Influence of Draft Tube Shape on Surging Characteristics of Reaction Turbines," *Report No. REC-ERC-72-24*, U. S. Bureau of Reclamation, July 1972.
- Palde, U. J., "Model and Prototype Turbine Draft Tube Surge Analysis by the Swirl Momentum Method," *Proceedings*, 7th Symposium of the International Association for Hydraulic Research Section for Hydraulic Machinery Equipment and Cavitation, Vienna, Austria, Sept. 1974.
- Rheingans, W. J., "Power Swings in Hydroelectric Power Plants," *Transactions of the ASME*, Vol. 62, No. 174, Apr. 1940, pp. 171-184.

- Ruud, F. O., "Initial Operation of 600-MW Turbines at Grand Coulee Third Powerplant," *Proceedings*, 8th Symposium of the International Association for Hydraulic Research Section for Hydraulic Machinery Equipment and Cavitation, Leningrad, USSR, Sept. 1976, pp. 502-515.
- Sarpkaya, T., "On Stationary and Travelling Vortex Breakdowns," *Journal of Fluid Mechanics*, Vol. 45, 1971, pp. 545-559.
- Seybert, T. A., W. S. Gearhart, and H. T. Falvey, "Studies of a Method To Prevent Draft Tube Surge in Pump-Turbines," *Proceedings*, Joint Symposium on Design and Operation of Fluid Machinery, Fort Collins, Colorado, June 1978, pp. 151-166.
- "Symposium on the Grand Coulee Third Power Plant," *Proceedings*, The American Power Conference, Vol. 39, Chicago, Illinois, Apr. 1977, pp. 968-970.
- Ulith, P., "A Contribution to Influencing the Part-Load Behavior of Francis Turbines by Aeration and σ -Value," *Proceedings*, 4th Symposium of the International Association for Hydraulic Research Section for Hydraulic Machinery Equipment and Cavitation, Paper B1, Lausanne, Switzerland, 1968.
- U. S. Bureau of Reclamation, "Designer's Operating Criteria - Turbine Model Test Facility at Estes Powerplant," Denver, Colorado, Aug. 1974.
- Warnick, C. C., H. A. Mayo, Jr., J. L. Carson, and L. H. Sheldon, *Hydropower Engineering*, Prentice-Hall, Inc., Englewood Cliffs, New Jersey, 326 pp.
- Yocum, A. M., "Analysis of the Flow Through Turbine Wicket Gates with an Application to the Prediction of Draft Tube Surge," *Proceedings*, Joint Symposium on Design and Operation of Fluid Machinery, Fort Collins, Colorado, June 1978, pp. 121-139.

APPENDIX A
PRESSURE FLUCTUATION DATA

Table A-1. Dominant pressure fluctuation data used for analysis. Shaded lines indicate test points where a twin vortex was observed.

Run	Gate (deg)	H (ft)	N (rpm)	Q (cfs)	T (ft-lb)	\bar{U}	Eff	ϕ_2	HP ₁₁	Swirl Param	f (Hz)	TRANSDUCER LOCATION - T1			
												RMS amp. (dBV)	(psi)	Freq. Param	Press Param
2-7	36.2	103.4	2982	12.68	134	0.457	0.51	1.41	0.133	0.52	15.5	-21.74	1.64	0.60	0.29
2-8	36.2	100.3	2889	12.80	159	0.493	0.60	1.39	0.160	0.46	13.5	-24.40	1.21	0.52	0.21
3-7	30.2	122.0	2671	12.76	288	0.381	0.83	1.17	0.200	0.34	12.5	-36.23	0.31	0.48	0.05
3-8	30.2	123.1	2878	12.71	248	0.369	0.77	1.25	0.183	0.43	12.5	-25.76	1.03	0.48	0.18
4-5	26.2	113.3	2361	10.93	270	0.407	0.86	1.07	0.185	0.33	12.0	-30.59	0.59	0.54	0.14
4-6	26.2	113.6	2662	10.91	213	0.405	0.77	1.20	0.164	0.52	11.0	-24.90	1.14	0.49	0.27
4-7	26.2	112.8	2891	10.76	167	0.430	0.67	1.31	0.141	0.67	11.5	-19.88	2.03	0.52	0.50
5-3	23.2	114.6	2144	10.07	277	0.402	0.86	0.97	0.169	0.33	10.5	-31.97	0.50	0.51	0.14
5-4	23.2	114.9	2253	10.14	264	0.398	0.86	1.01	0.169	0.40	10.5	-29.00	0.71	0.51	0.20
5-5	23.2	115.9	2509	10.03	222	0.395	0.80	1.12	0.156	0.55	10.0	-25.50	1.06	0.49	0.30
5-7	23.2	116.4	2777	9.96	180	0.395	0.72	1.24	0.139	0.71	11.0	-21.02	1.78	0.54	0.51
6-4	20.2	115.6	1967	9.21	273	0.401	0.85	0.88	0.151	0.39	9.0	-31.43	0.54	0.48	0.18
6-5	20.2	117.2	2234	9.12	229	0.392	0.80	0.99	0.141	0.58	8.5	-25.94	1.01	0.46	0.35
6-6	20.2	116.8	2440	8.99	201	0.410	0.78	1.09	0.136	0.69	9.0	-24.68	1.17	0.49	0.41
6-7	20.2	118.4	2706	8.91	166	0.401	0.72	1.20	0.122	0.85	10.0	-22.98	1.42	0.55	0.51
7-4	17.2	117.4	1855	8.26	257	0.376	0.83	0.83	0.131	0.53	7.5	-32.31	0.49	0.44	0.20
7-5	17.2	119.6	2060	8.24	235	0.357	0.83	0.91	0.129	0.65	8.0	-27.75	0.82	0.48	0.35
7-6	17.2	119.4	2286	8.05	199	0.387	0.79	1.01	0.122	0.81	8.5	-26.06	1.00	0.52	0.44
7-7	17.2	121.3	2525	7.88	160	0.392	0.71	1.10	0.106	1.01	9.0	-24.46	1.20	0.56	0.55
7-8	17.2	120.5	2590	7.91	151	0.397	0.69	1.14	0.103	1.08	9.5	-22.75	1.46	0.59	0.67
8-4	15.2	115.9	1773	7.61	226	0.381	0.76	0.79	0.112	0.79	7.5	-31.45	0.54	0.48	0.26
8-5	15.2	118.0	2015	7.56	208	0.370	0.79	0.89	0.114	0.90	7.5	-28.26	0.77	0.49	0.39
8-6	15.2	121.5	2239	7.36	177	0.354	0.74	0.98	0.103	1.05	8.0	-31.91	0.51	0.53	0.27
8-7	15.2	122.2	2378	7.37	157	0.351	0.70	1.04	0.097	1.20	21.5	-30.30	0.61	1.43	0.32
9-3	13.2	126.9	1960	7.09	201	0.341	0.74	0.84	0.096	1.18	8.0	-27.66	0.83	0.55	0.47
9-4	13.2	124.8	2113	6.95	172	0.397	0.70	0.91	0.091	1.36	7.5	-30.09	0.63	0.53	0.37
9-5	13.2	128.8	2342	6.92	150	0.356	0.66	0.99	0.084	1.54	21.0	-30.86	0.57	1.48	0.34
9-6	13.2	131.6	2658	6.75	103	0.351	0.52	1.12	0.063	1.89	32.0	-33.39	0.43	2.32	0.27
10-3	9.2	114.4	1601	5.43	137	0.399	0.59	0.72	0.063	2.41	9.0	-37.80	0.26	0.81	0.25
10-4	9.2	114.6	1684	5.45	129	0.398	0.58	0.76	0.062	2.54	8.0	-32.06	0.50	0.72	0.48
10-5	9.2	115.4	1845	5.39	110	0.400	0.55	0.83	0.057	2.76	8.5	-32.82	0.46	0.77	0.45
10-6	9.2	116.3	1968	5.38	101	0.396	0.53	0.88	0.055	2.88	19.0	-33.81	0.41	1.73	0.40
10-7	9.2	118.2	2101	5.32	90	0.385	0.51	0.93	0.051	3.01	19.5	-36.15	0.31	1.79	0.32
10-8	9.2	119.7	2234	5.34	76	0.378	0.45	0.98	0.045	3.22	28.0	-36.45	0.30	2.57	0.30
11-3	11.2	119.0	1685	6.20	172	0.384	0.66	0.74	0.078	1.59	8.0	-34.70	0.37	0.63	0.27
11-4	11.2	120.0	1852	6.19	155	0.379	0.65	0.81	0.076	1.77	7.5	-29.13	0.70	0.59	0.52
11-5	11.2	122.7	2120	6.11	132	0.366	0.63	0.92	0.072	1.97	7.5	-30.98	0.57	0.60	0.43
11-6	11.2	123.2	2249	6.11	118	0.364	0.59	0.98	0.068	2.13	19.5	-29.04	0.71	1.56	0.54
12-3	13.2	120.5	1749	6.98	202	0.387	0.71	0.77	0.093	1.13	7.5	-32.65	0.47	0.53	0.27
12-4	13.2	125.1	2214	6.80	152	0.364	0.66	0.95	0.084	1.47	8.0	-31.65	0.52	0.58	0.32
12-5	13.2	125.8	2429	6.74	127	0.369	0.61	1.04	0.076	1.67	21.0	-30.29	0.61	1.52	0.39
13-1	10.2	120.2	1629	5.87	161	0.407	0.62	0.72	0.070	1.91	8.0	-38.78	0.23	0.67	0.19
13-2	10.2	122.1	1796	5.90	147	0.383	0.62	0.78	0.068	2.09	7.5	-30.55	0.59	0.62	0.49
13-3	10.2	123.1	1924	5.81	134	0.377	0.61	0.84	0.066	2.20	8.5	-28.64	0.74	0.72	0.63
13-4	10.2	123.9	2023	5.79	127	0.373	0.60	0.88	0.065	2.27	8.0	-30.65	0.59	0.68	0.50
13-5	10.2	124.1	2064	5.80	123	0.372	0.59	0.89	0.064	2.32	8.0	-30.03	0.63	0.67	0.54
13-5	10.2	124.1	2064	5.80	123	0.372	0.59	0.89	0.064	2.32	20.0	-31.42	0.54	1.69	0.46
13-6	10.2	124.4	2160	5.77	114	0.371	0.58	0.93	0.062	2.42	19.5	-31.12	0.56	1.65	0.48
13-7	10.2	126.5	2265	5.70	102	0.361	0.54	0.97	0.057	2.53	20.0	-34.65	0.37	1.72	0.33
14-1	12.2	120.1	1705	6.56	192	0.399	0.70	0.75	0.087	1.27	7.5	-34.94	0.36	0.56	0.24
14-2	12.2	120.4	1831	6.53	176	0.397	0.69	0.80	0.085	1.41	7.5	-28.75	0.73	0.56	0.49
14-3	12.2	122.3	2017	6.47	163	0.387	0.70	0.88	0.085	1.50	8.0	-28.29	0.77	0.61	0.53
14-4	12.2	124.3	2227	6.41	137	0.377	0.64	0.96	0.077	1.73	20.0	-31.48	0.53	1.53	0.37
15-1	14.2	117.2	1784	7.23	212	0.399	0.75	0.79	0.104	0.93	7.5	-31.27	0.55	0.51	0.30
15-2	14.2	119.3	2017	7.12	196	0.388	0.78	0.89	0.106	1.01	7.5	-29.04	0.71	0.52	0.40
15-3	14.2	123.3	2355	7.01	148	0.368	0.68	1.02	0.089	1.35	21.5	-31.34	0.54	1.50	0.32
16-1	15.2	119.8	2491	7.14	130	0.386	0.64	1.10	0.086	1.34	21.5	-31.95	0.51	1.47	0.28
17-1	16.2	113.1	1785	7.73	233	0.448	0.80	0.81	0.121	0.62	7.0	-31.95	0.51	0.44	0.24
17-2	16.2	115.2	2019	7.65	211	0.435	0.81	0.91	0.120	0.74	7.5	-28.23	0.78	0.48	0.38
17-3	16.2	118.8	2255	7.55	178	0.413	0.75	1.00	0.108	0.94	8.0	-30.11	0.63	0.52	0.31

Table A-2. All recorded model test data. Shaded lines indicate test points at which the amplitude of pressure fluctuations was higher at T2 than at T1 (observed in the comparison of simultaneous time-domain signals recorded using the oscilloscope).

Run	Gate (deg)	H (ft)	N (rpm)	Q (cfs)	T (ft-lb)	σ	Eff	ϕ_2	HP ₁₁	Swirl Param	TRANSDUCER LOCATION - T1					Shaft Freq.
											f (Hz)	RMS amp. (dBV)	(psi)	Freq. Param	Press Param	
Trial 19.7	172	2570	10.73	361	0.173	0.85	0.95	0.144	0.47	11.0	-24.27	1.22	0.50	0.30		42.8
Trial 19.7	172	2570	10.73	361	0.173	0.85	0.95	0.144	0.47	21.5	-40.61	0.19	0.98	0.05		42.8
Trial 19.7	157	2992	9.92	222	0.258	0.71	1.15	0.118	0.83	11.0	-19.56	2.11	0.54	0.61		49.9
Trial 19.7	158	3002	10.04	236	0.187	0.75	1.15	0.124	0.80	11.0	-19.90	2.03	0.54	0.57		50.0
Trial 13.6	183	2210	8.36	318	0.161	0.77	0.79	0.099	0.87	9.0	-25.73	1.04	0.53	0.42		36.8
2-1	36.2	134	2040	14.91	504	0.224	0.87	0.85	0.232	-0.07						34.0
2-2	36.2	121	1872	14.12	459	0.408	0.85	0.82	0.227	-0.08						31.2
2-3	36.2	121	2180	14.11	403	0.407	0.86	0.96	0.231	0.03						36.3
2-4	36.2	120	2383	14.18	367	0.410	0.86	1.05	0.232	0.11						39.7
2-5	36.2	120	2720	14.33	311	0.403	0.82	1.20	0.224	0.24						45.3
2-6	36.2	115	2957	13.78	221	0.418	0.69	1.33	0.185	0.38						49.3
2-7	36.2	103	2982	12.68	134	0.457	0.51	1.41	0.133	0.52	15.5	-21.74	1.64	0.60	0.29	49.7
2-7	36.2	103	2982	12.68	134	0.457	0.51	1.41	0.133	0.52	4.5	-37.24	0.28	0.17	0.05	49.7
2-7	36.2	103	2982	12.68	134	0.457	0.51	1.41	0.133	0.52	28.0	-32.72	0.46	1.08	0.08	49.7
2-7	36.2	103	2982	12.68	134	0.457	0.51	1.41	0.133	0.52	50.0	-40.34	0.19	1.93	0.03	49.7
2-7	36.2	103	2982	12.68	134	0.457	0.51	1.41	0.133	0.52	80.0	-29.04	0.71	3.09	0.13	49.7
2-8	36.2	100	2889	12.80	159	0.493	0.60	1.39	0.160	0.46	13.5	-24.40	1.21	0.52	0.21	48.2
2-8	36.2	100	2889	12.80	159	0.493	0.60	1.39	0.160	0.46	3.5	-38.98	0.23	0.13	0.04	48.2
2-8	36.2	100	2889	12.80	159	0.493	0.60	1.39	0.160	0.46	27.5	-36.27	0.31	1.05	0.05	48.2
2-8	36.2	100	2889	12.80	159	0.493	0.60	1.39	0.160	0.46	34.5	-31.66	0.52	1.32	0.09	48.2
2-8	36.2	100	2889	12.80	159	0.493	0.60	1.39	0.160	0.46	48.0	-42.91	0.14	1.83	0.03	48.2
2-8	36.2	100	2889	12.80	159	0.493	0.60	1.39	0.160	0.46	96.0	-36.26	0.31	3.67	0.05	48.2
3-1	30.2	119	1530	12.75	476	0.411	0.81	0.68	0.197	-0.13						25.5
3-2	30.2	128	1587	13.27	527	0.276	0.83	0.68	0.202	-0.16						26.5
3-3	30.2	121	1759	12.82	454	0.389	0.87	0.77	0.211	-0.06						29.3
3-4	30.2	121	1910	12.78	424	0.386	0.88	0.84	0.212	0.00						31.8
3-5	30.2	122	2236	12.79	374	0.376	0.90	0.98	0.218	0.13						37.3
3-6	30.2	123	2488	12.79	329	0.369	0.88	1.08	0.211	0.24						41.5
3-7	30.2	122	2671	12.76	288	0.381	0.83	1.17	0.200	0.34	12.5	-36.23	0.31	0.48	0.05	44.5
3-7	30.2	122	2671	12.76	288	0.381	0.83	1.17	0.200	0.34	3.0	-38.20	0.25	0.12	0.04	44.5
3-7	30.2	122	2671	12.76	288	0.381	0.83	1.17	0.200	0.34	35.0	-36.95	0.28	1.34	0.05	44.5
3-8	30.2	123	2878	12.71	248	0.369	0.77	1.25	0.183	0.43	12.5	-25.76	1.03	0.48	0.18	48.0
3-8	30.2	123	2878	12.71	248	0.369	0.77	1.25	0.183	0.43	3.5	-37.77	0.26	0.13	0.05	48.0
3-8	30.2	123	2878	12.71	248	0.369	0.77	1.25	0.183	0.43	25.0	-32.61	0.47	0.96	0.08	48.0
3-8	30.2	123	2878	12.71	248	0.369	0.77	1.25	0.183	0.43	48.0	-43.94	0.13	1.85	0.02	48.0
3-9	30.2	125	2900	12.91	260	0.247	0.79	1.25	0.189	0.42	12.5	-26.80	0.92	0.47	0.16	48.3
4-1	26.2	118	1739	11.47	399	0.376	0.86	0.77	0.190	0.02						29.0
4-2	26.2	116	1917	11.43	373	0.393	0.90	0.86	0.199	0.09						32.0
4-3	26.2	116	2106	11.35	326	0.398	0.87	0.94	0.191	0.22						35.1
4-4	26.2	115	2263	11.01	288	0.373	0.87	1.02	0.185	0.29	37.5	-38.41	0.24	1.67	0.06	37.7
4-5	26.2	113	2361	10.93	270	0.407	0.86	1.07	0.185	0.33	12.0	-30.59	0.59	0.54	0.14	39.4
4-5	26.2	113	2361	10.93	270	0.407	0.86	1.07	0.185	0.33	27.5	-39.71	0.21	1.23	0.05	39.4
4-5	26.2	113	2361	10.93	270	0.407	0.86	1.07	0.185	0.33	39.5	-43.25	0.14	1.77	0.03	39.4
4-6	26.2	114	2662	10.91	213	0.405	0.77	1.20	0.164	0.52	11.0	-24.90	1.14	0.49	0.27	44.4
4-6	26.2	114	2662	10.91	213	0.405	0.77	1.20	0.164	0.52	33.5	-40.03	0.20	1.50	0.05	44.4
4-7	26.2	113	2891	10.76	167	0.430	0.67	1.31	0.141	0.67	11.5	-19.88	2.03	0.52	0.50	48.2
4-7	26.2	113	2891	10.76	167	0.430	0.67	1.31	0.141	0.67	23.0	-24.05	1.26	1.05	0.31	48.2
4-8	26.2	112	2893	10.90	180	0.294	0.72	1.32	0.153	0.64	11.5	-19.50	2.12	0.52	0.51	48.2
4-8	26.2	112	2893	10.90	180	0.294	0.72	1.32	0.153	0.64	23.5	-39.83	0.20	1.05	0.05	48.2
4-8	26.2	112	2893	10.90	180	0.294	0.72	1.32	0.153	0.64	48.5	-43.99	0.13	2.18	0.03	48.2
5-1	23.2	113	1480	10.34	375	0.398	0.80	0.67	0.162	0.02						24.7
5-2	23.2	112	1820	10.26	332	0.420	0.89	0.83	0.179	0.16						30.3
5-3	23.2	115	2144	10.07	277	0.402	0.86	0.97	0.169	0.33	10.5	-31.97	0.50	0.51	0.14	35.7
5-3	23.2	115	2144	10.07	277	0.402	0.86	0.97	0.169	0.33	25.0	-45.90	0.10	1.21	0.03	35.7
5-3	23.2	115	2144	10.07	277	0.402	0.86	0.97	0.169	0.33	36.0	-43.03	0.14	1.75	0.04	35.7
5-4	23.2	115	2253	10.14	264	0.398	0.86	1.01	0.169	0.40	10.5	-29.00	0.71	0.51	0.20	37.6
5-4	23.2	115	2253	10.14	264	0.398	0.86	1.01	0.169	0.40	20.0	-36.95	0.28	0.97	0.08	37.6
5-4	23.2	115	2253	10.14	264	0.398	0.86	1.01	0.169	0.40	37.5	-50.13	0.06	1.81	0.02	37.6
5-4	23.2	115	2253	10.14	264	0.398	0.86	1.01	0.169	0.40	64.5	-53.16	0.04	3.11	0.01	37.6
5-4	23.2	115	2253	10.14	264	0.398	0.86	1.01	0.169	0.40	75.5	-57.79	0.03	3.64	0.01	37.6
5-5	23.2	116	2509	10.03	222	0.395	0.80	1.12	0.156	0.55	10.0	-25.50	1.06	0.49	0.30	41.8
5-5	23.2	116	2509	10.03	222	0.395	0.80	1.12	0.156	0.55	20.5	-46.32	0.10	1.00	0.03	41.8
5-6	23.2	125	2588	10.54	254	0.244	0.84	1.12	0.165	0.52	10.5	-22.84	1.44	0.49	0.37	43.1
5-6	23.2	125	2588	10.54	254	0.244	0.84	1.12	0.165	0.52	21.0	-39.31	0.22	0.97	0.06	43.1
5-6	23.2	125	2588	10.54	254	0.244	0.84	1.12	0.165	0.52	43.0	-45.27	0.11	2.00	0.03	43.1
5-6	23.2	125	2588	10.54	254	0.244	0.84	1.12	0.165	0.52	86.0	-53.65	0.04	3.99	0.01	43.1
5-7	23.2	116	2777	9.96	180	0.395	0.72	1.24	0.139	0.71	11.0	-21.02	1.78	0.54	0.51	46.3
5-7	23.2	116	2777	9.96	180	0.395	0.72	1.24	0.139	0.71	21.5	-33.79	0.41	1.06	0.12	46.3
5-8	23.2	125	2783	10.46	219	0.242	0.78	1.20	0.152	0.63	10.5	-23.95	1.27	0.49	0.33	46.4
5-9	23.2	114	2903	9.82	162	0.264	0.70	1.31	0.135	0.76	11.5	-17.79	2.58	0.57	0.77	48.4

Table A-2 [continued]. All model test data.

Run	Gate (deg)	H (ft)	N (rpm)	Q (cfs)	T (ft-lb)	σ	Eff	ϕ_2	HP ₁₁	Swirl Param	TRANSDUCER LOCATION - T1					Press Param	Shaft Freq.
											f (Hz)	RMS amp. (dBV)	(psi)	Freq. Param			
6-1	20.2	115	1322	9.27	353	0.407	0.74	0.60	0.133	0.03							22.0
6-2	20.2	113	1531	9.30	322	0.415	0.79	0.69	0.143	0.19							25.5
6-3	20.2	114	1803	9.30	297	0.405	0.85	0.81	0.153	0.31							30.1
6-4	20.2	116	1967	9.21	273	0.401	0.85	0.88	0.151	0.39	9.0	-31.43	0.54	0.48	0.18		32.8
6-4	20.2	116	1967	9.21	273	0.401	0.85	0.88	0.151	0.39	18.0	-46.34	0.10	0.96	0.03		32.8
6-4	20.2	116	1967	9.21	273	0.401	0.85	0.88	0.151	0.39	24.0	-47.31	0.09	1.28	0.03		32.8
6-4	20.2	116	1967	9.21	273	0.401	0.85	0.88	0.151	0.39	65.5	-55.74	0.03	3.48	0.01		32.8
6-5	20.2	117	2234	9.12	229	0.392	0.80	0.99	0.141	0.58	8.5	-25.94	1.01	0.46	0.35		37.2
6-5	20.2	117	2234	9.12	229	0.392	0.80	0.99	0.141	0.58	17.0	-33.66	0.42	0.91	0.14		37.2
6-6	20.2	117	2440	8.99	201	0.410	0.78	1.09	0.136	0.69	9.0	-24.68	1.17	0.49	0.41		40.7
6-6	20.2	117	2440	8.99	201	0.410	0.78	1.09	0.136	0.69	18.5	-32.89	0.45	1.01	0.16		40.7
6-6	20.2	117	2440	8.99	201	0.410	0.78	1.09	0.136	0.69	27.0	-44.65	0.12	1.47	0.04		40.7
6-6	20.2	117	2440	8.99	201	0.410	0.78	1.09	0.136	0.69	41.0	-42.84	0.14	2.23	0.05		40.7
6-6	20.2	117	2440	8.99	201	0.410	0.78	1.09	0.136	0.69	81.0	-55.00	0.04	4.41	0.01		40.7
6-7	20.2	118	2706	8.91	166	0.401	0.72	1.20	0.122	0.85	10.0	-22.98	1.42	0.55	0.51		45.1
6-7	20.2	118	2706	8.91	166	0.401	0.72	1.20	0.122	0.85	20.0	-39.51	0.21	1.10	0.08		45.1
6-7	20.2	118	2706	8.91	166	0.401	0.72	1.20	0.122	0.85	45.0	-41.95	0.16	2.47	0.06		45.1
7-1	17.2	115	1350	8.18	309	0.421	0.75	0.61	0.118	0.18							22.5
7-2	17.2	116	1578	8.34	286	0.383	0.78	0.71	0.126	0.39							26.3
7-3	17.2	117	1803	8.32	260	0.378	0.81	0.80	0.129	0.53							30.1
7-4	17.2	117	1855	8.26	257	0.376	0.83	0.83	0.131	0.53	7.5	-32.31	0.49	0.44	0.20		30.9
7-4	17.2	117	1855	8.26	257	0.376	0.83	0.83	0.131	0.53	15.0	-47.58	0.08	0.89	0.04		30.9
7-4	17.2	117	1855	8.26	257	0.376	0.83	0.83	0.131	0.53	23.0	-52.23	0.05	1.36	0.02		30.9
7-4	17.2	117	1855	8.26	257	0.376	0.83	0.83	0.131	0.53	38.5	-51.75	0.05	2.28	0.02		30.9
7-5	17.2	120	2060	8.24	235	0.357	0.83	0.91	0.129	0.65	8.0	-27.75	0.82	0.48	0.35		34.3
7-5	17.2	120	2060	8.24	235	0.357	0.83	0.91	0.129	0.65	15.5	-31.94	0.51	0.92	0.21		34.3
7-5	17.2	120	2060	8.24	235	0.357	0.83	0.91	0.129	0.65	23.0	-43.91	0.13	1.37	0.05		34.3
7-6	17.2	119	2286	8.05	199	0.387	0.79	1.01	0.122	0.81	8.5	-26.06	1.00	0.52	0.44		38.1
7-6	17.2	119	2286	8.05	199	0.387	0.79	1.01	0.122	0.81	16.5	-39.87	0.20	1.00	0.09		38.1
7-6	17.2	119	2286	8.05	199	0.387	0.79	1.01	0.122	0.81	25.0	-50.66	0.06	1.52	0.03		38.1
7-6	17.2	119	2286	8.05	199	0.387	0.79	1.01	0.122	0.81	38.0	-43.84	0.13	2.31	0.06		38.1
7-6	17.2	119	2286	8.05	199	0.387	0.79	1.01	0.122	0.81	76.5	-52.06	0.05	4.65	0.02		38.1
7-7	17.2	121	2525	7.88	160	0.392	0.71	1.10	0.106	1.01	9.0	-24.46	1.20	0.56	0.55		42.1
7-7	17.2	121	2525	7.88	160	0.392	0.71	1.10	0.106	1.01	18.0	-36.39	0.30	1.12	0.14		42.1
7-7	17.2	121	2525	7.88	160	0.392	0.71	1.10	0.106	1.01	42.5	-41.48	0.17	2.64	0.08		42.1
7-8	17.2	121	2590	7.91	151	0.397	0.69	1.14	0.103	1.08	9.5	-22.75	1.46	0.59	0.67		43.2
7-8	17.2	121	2590	7.91	151	0.397	0.69	1.14	0.103	1.08	19.0	-37.43	0.27	1.18	0.12		43.2
7-8	17.2	121	2590	7.91	151	0.397	0.69	1.14	0.103	1.08	43.0	-39.68	0.21	2.66	0.10		43.2
7-9	17.2	124	2768	7.75	118	0.376	0.57	1.20	0.082	1.26							46.1
8-1	15.2	116	1346	7.60	281	0.380	0.72	0.60	0.106	0.40							22.4
8-2	15.2	116	1573	7.61	252	0.383	0.76	0.71	0.111	0.61							26.2
8-3	15.2	116	1599	7.61	252	0.383	0.77	0.72	0.113	0.61							26.7
8-4	15.2	116	1773	7.61	226	0.381	0.76	0.79	0.112	0.79	7.5	-31.45	0.54	0.48	0.26		29.6
8-4	15.2	116	1773	7.61	226	0.381	0.76	0.79	0.112	0.79	15.0	-42.87	0.14	0.96	0.07		29.6
8-4	15.2	116	1773	7.61	226	0.381	0.76	0.79	0.112	0.79	22.0	-48.26	0.08	1.41	0.04		29.6
8-4	15.2	116	1773	7.61	226	0.381	0.76	0.79	0.112	0.79	30.0	-49.25	0.07	1.93	0.03		29.6
8-4	15.2	116	1773	7.61	226	0.381	0.76	0.79	0.112	0.79	59.5	-53.47	0.04	3.83	0.02		29.6
8-5	15.2	118	2015	7.56	208	0.370	0.79	0.89	0.114	0.90	7.5	-28.26	0.77	0.49	0.39		33.6
8-5	15.2	118	2015	7.56	208	0.370	0.79	0.89	0.114	0.90	33.5	-49.08	0.07	2.17	0.04		33.6
8-5	15.2	118	2015	7.56	208	0.370	0.79	0.89	0.114	0.90	67.0	-54.90	0.04	4.34	0.02		33.6
8-6	15.2	122	2239	7.36	177	0.354	0.74	0.98	0.103	1.05	8.0	-31.91	0.51	0.53	0.27		37.3
8-6	15.2	122	2239	7.36	177	0.354	0.74	0.98	0.103	1.05	15.0	-35.62	0.33	1.00	0.18		37.3
8-6	15.2	122	2239	7.36	177	0.354	0.74	0.98	0.103	1.05	23.0	-38.23	0.25	1.53	0.13		37.3
8-6	15.2	122	2239	7.36	177	0.354	0.74	0.98	0.103	1.05	37.0	-44.02	0.13	2.46	0.07		37.3
8-6	15.2	122	2239	7.36	177	0.354	0.74	0.98	0.103	1.05	74.5	-47.27	0.09	4.95	0.05		37.3
8-7	15.2	122	2378	7.37	157	0.351	0.70	1.04	0.097	1.20	21.5	-30.30	0.61	1.43	0.32		39.6
8-7	15.2	122	2378	7.37	157	0.351	0.70	1.04	0.097	1.20	43.0	-37.08	0.28	2.85	0.15		39.6
8-8	15.2	129	2424	7.58	179	0.236	0.74	1.03	0.103	1.11	22.5	-31.96	0.51	1.45	0.25		40.4
8-8	15.2	129	2424	7.58	179	0.236	0.74	1.03	0.103	1.11	9.0	-33.61	0.42	0.58	0.21		40.4
8-8	15.2	129	2424	7.58	179	0.236	0.74	1.03	0.103	1.11	14.5	-35.59	0.33	0.94	0.17		40.4
8-9	15.2	131	2640	7.52	147	0.232	0.66	1.11	0.090	1.32	22.5	-28.39	0.76	1.46	0.39		44.0
8-9	15.2	131	2640	7.52	147	0.232	0.66	1.11	0.090	1.32	45.0	-36.64	0.29	2.93	0.15		44.0
8-10	15.2	132	2845	7.34	104	0.252	0.51	1.19	0.068	1.59	34.5	-31.46	0.54	2.30	0.28		47.4
9-1	13.2	132	1515	7.37	286	0.255	0.75	0.64	0.100	0.67							25.3
9-2	13.2	132	1751	7.32	248	0.254	0.76	0.74	0.100	0.93							29.2
9-3	13.2	127	1960	7.09	201	0.341	0.74	0.84	0.096	1.18	8.0	-27.66	0.83	0.55	0.47		32.7
9-3	13.2	127	1960	7.09	201	0.341	0.74	0.84	0.096	1.18	16.5	-44.87	0.11	1.14	0.07		32.7
9-3	13.2	127	1960	7.09	201	0.341	0.74	0.84	0.096	1.18	24.5	-49.03	0.07	1.69	0.04		32.7
9-4	13.2	125	2113	6.95	172	0.397	0.70	0.91	0.091	1.36	7.5	-30.09	0.63	0.53	0.37		35.2
9-4	13.2	125	2113	6.95	172	0.397	0.70	0.91	0.091	1.36	15.5	-38.16	0.25	1.09	0.15		35.2
9-4	13.2	125	2113	6.95	172	0.397	0.70	0.91	0.091	1.36	23.0	-45.81	0.10	1.62	0.06		35.2

Table A-2 [continued]. All model test data.

Run	Gate (deg)	H (ft)	N (rpm)	Q (cfs)	T (ft-lb)	σ	Eff	ϕ_2	HP ₁₁	TRANSDUCER LOCATION - T1						
										Swirl Param	f (Hz)	RMS amp. (dBV)	(psi)	Freq. Param	Press Param	Shaft Freq.
9-5	13.2	129	2342	6.92	150	0.356	0.66	0.99	0.084	1.54	21.0	-30.86	0.57	1.48	0.34	39.0
9-5	13.2	129	2342	6.92	150	0.356	0.66	0.99	0.084	1.54	39.0	-37.43	0.27	2.76	0.16	39.0
9-5	13.2	129	2342	6.92	150	0.356	0.66	0.99	0.084	1.54	41.5	-39.56	0.21	2.93	0.13	39.0
9-6	13.2	132	2658	6.75	103	0.351	0.52	1.12	0.063	1.89	32.0	-33.39	0.43	2.32	0.27	44.3
9-6	13.2	132	2658	6.75	103	0.351	0.52	1.12	0.063	1.89	17.5	-34.06	0.40	1.27	0.25	44.3
9-6	13.2	132	2658	6.75	103	0.351	0.52	1.12	0.063	1.89	44.5	-35.46	0.34	3.23	0.21	44.3
9-7	13.2	133	2848	6.69	72	0.354	0.39	1.19	0.047	2.16						47.5
10-1	9.2	111	1332	5.42	162	0.433	0.60	0.61	0.065	2.06						22.2
10-2	9.2	114	1564	5.39	139	0.411	0.60	0.71	0.063	2.36						26.1
10-3	9.2	114	1601	5.43	137	0.399	0.59	0.72	0.063	2.41	9.0	-37.80	0.26	0.81	0.25	26.7
10-3	9.2	114	1601	5.43	137	0.399	0.59	0.72	0.063	2.41	18.0	-48.13	0.08	1.62	0.08	26.7
10-4	9.2	115	1684	5.45	129	0.398	0.58	0.76	0.062	2.54	8.0	-32.06	0.50	0.72	0.48	28.1
10-4	9.2	115	1684	5.45	129	0.398	0.58	0.76	0.062	2.54	16.5	-44.27	0.12	1.48	0.12	28.1
10-5	9.2	115	1845	5.39	110	0.400	0.55	0.83	0.057	2.76	8.5	-32.82	0.46	0.77	0.45	30.8
10-5	9.2	115	1845	5.39	110	0.400	0.55	0.83	0.057	2.76	17.0	-40.54	0.19	1.54	0.19	30.8
10-6	9.2	116	1968	5.38	101	0.396	0.53	0.88	0.055	2.88	19.0	-33.81	0.41	1.73	0.40	32.8
10-6	9.2	116	1968	5.38	101	0.396	0.53	0.88	0.055	2.88	10.5	-38.99	0.22	0.95	0.22	32.8
10-6	9.2	116	1968	5.38	101	0.396	0.53	0.88	0.055	2.88	33.0	-43.58	0.13	3.00	0.13	32.8
10-6	9.2	116	1968	5.38	101	0.396	0.53	0.88	0.055	2.88	38.5	-40.59	0.19	3.50	0.18	32.8
10-6	9.2	116	1968	5.38	101	0.396	0.53	0.88	0.055	2.88	51.5	-41.37	0.17	4.68	0.17	32.8
10-7	9.2	118	2101	5.32	90	0.385	0.51	0.93	0.051	3.01	19.5	-36.15	0.31	1.79	0.32	35.0
10-7	9.2	118	2101	5.32	90	0.385	0.51	0.93	0.051	3.01	12.5	-39.47	0.21	1.15	0.22	35.0
10-7	9.2	118	2101	5.32	90	0.385	0.51	0.93	0.051	3.01	28.0	-40.55	0.19	2.58	0.19	35.0
10-7	9.2	118	2101	5.32	90	0.385	0.51	0.93	0.051	3.01	39.0	-43.84	0.13	3.59	0.13	35.0
10-7	9.2	118	2101	5.32	90	0.385	0.51	0.93	0.051	3.01	53.5	-44.68	0.12	4.92	0.12	35.0
10-7	9.2	118	2101	5.32	90	0.385	0.51	0.93	0.051	3.01	61.5	-44.66	0.12	5.66	0.12	35.0
10-8	9.2	120	2234	5.34	76	0.378	0.45	0.98	0.045	3.22	28.0	-36.45	0.30	2.57	0.30	37.2
10-8	9.2	120	2234	5.34	76	0.378	0.45	0.98	0.045	3.22	16.0	-38.31	0.24	1.47	0.24	37.2
10-9	9.2	121	2423	5.27	57	0.371	0.36	1.06	0.036	3.47	40.5	-34.66	0.37	3.76	0.38	40.4
11-1	11.2	117	1362	6.29	209	0.395	0.65	0.61	0.079	1.26						22.7
11-2	11.2	118	1526	6.24	197	0.389	0.68	0.68	0.082	1.36						25.4
11-3	11.2	119	1685	6.20	172	0.384	0.66	0.74	0.078	1.59	8.0	-34.70	0.37	0.63	0.27	28.1
11-3	11.2	119	1685	6.20	172	0.384	0.66	0.74	0.078	1.59	14.5	-43.60	0.13	1.14	0.10	28.1
11-4	11.2	120	1852	6.19	155	0.379	0.65	0.81	0.076	1.77	7.5	-29.13	0.70	0.59	0.52	30.9
11-4	11.2	120	1852	6.19	155	0.379	0.65	0.81	0.076	1.77	15.0	-42.83	0.14	1.19	0.11	30.9
11-4	11.2	120	1852	6.19	155	0.379	0.65	0.81	0.076	1.77	23.0	-46.51	0.09	1.82	0.07	30.9
11-4	11.2	120	1852	6.19	155	0.379	0.65	0.81	0.076	1.77	32.0	-48.35	0.08	2.53	0.06	30.9
11-4	11.2	120	1852	6.19	155	0.379	0.65	0.81	0.076	1.77	38.5	-46.55	0.09	3.04	0.07	30.9
11-4	11.2	120	1852	6.19	155	0.379	0.65	0.81	0.076	1.77	50.0	-47.15	0.09	3.95	0.07	30.9
11-5	11.2	123	2120	6.11	132	0.366	0.63	0.92	0.072	1.97	7.5	-30.98	0.57	0.60	0.43	35.3
11-6	11.2	123	2249	6.11	118	0.364	0.59	0.98	0.068	2.13	19.5	-29.04	0.71	1.56	0.54	37.5
11-6	11.2	123	2249	6.11	118	0.364	0.59	0.98	0.068	2.13	39.0	-40.11	0.20	3.12	0.15	37.5
11-6	11.2	123	2249	6.11	118	0.364	0.59	0.98	0.068	2.13	53.0	-43.61	0.13	4.24	0.10	37.5
11-7	11.2	115	2426	5.81	74	0.417	0.45	1.09	0.051	2.52	40.0	-35.4	0.34	3.37	0.29	40.4
11-7	11.2	115	2426	5.81	74	0.417	0.45	1.09	0.051	2.52	17.0	-38.24	0.25	1.43	0.21	40.4
11-7	11.2	115	2426	5.81	74	0.417	0.45	1.09	0.051	2.52	29.0	-37.88	0.26	2.44	0.22	40.4
11-8	11.2	116	2638	5.74	46	0.407	0.31	1.18	0.034	2.84	44.0	-32.32	0.48	3.75	0.42	44.0
11-8	11.2	116	2638	5.74	46	0.407	0.31	1.18	0.034	2.84	5.0	-42.33	0.15	0.43	0.13	44.0
11-8	11.2	116	2638	5.74	46	0.407	0.31	1.18	0.034	2.84	22.0	-39.06	0.22	1.88	0.19	44.0
11-8	11.2	116	2638	5.74	46	0.407	0.31	1.18	0.034	2.84	27.5	-39.53	0.21	2.34	0.18	44.0
11-8	11.2	116	2638	5.74	46	0.407	0.31	1.18	0.034	2.84	36.5	-36.89	0.29	3.11	0.25	44.0
12-1	13.2	119	1370	7.03	249	0.393	0.68	0.60	0.092	0.76						22.8
12-2	13.2	120	1604	6.95	225	0.389	0.73	0.71	0.096	0.92						26.7
12-3	13.2	121	1749	6.98	202	0.387	0.71	0.77	0.093	1.13	7.5	-32.65	0.47	0.53	0.27	29.2
12-3	13.2	121	1749	6.98	202	0.387	0.71	0.77	0.093	1.13	15.0	-42.26	0.15	1.05	0.09	29.2
12-3	13.2	121	1749	6.98	202	0.387	0.71	0.77	0.093	1.13	22.5	-54.24	0.04	1.58	0.02	29.2
12-3	13.2	121	1749	6.98	202	0.387	0.71	0.77	0.093	1.13	29.5	-50.20	0.06	2.07	0.04	29.2
12-3	13.2	121	1749	6.98	202	0.387	0.71	0.77	0.093	1.13	37.5	-49.67	0.07	2.63	0.04	29.2
12-4	13.2	125	2214	6.80	152	0.364	0.66	0.95	0.084	1.47	8.0	-31.65	0.52	0.58	0.32	36.9
12-4	13.2	125	2214	6.80	152	0.364	0.66	0.95	0.084	1.47	16.0	-37.83	0.26	1.15	0.16	36.9
12-4	13.2	125	2214	6.80	152	0.364	0.66	0.95	0.084	1.47	24.0	-39.43	0.21	1.73	0.13	36.9
12-4	13.2	125	2214	6.80	152	0.364	0.66	0.95	0.084	1.47	36.5	-43.48	0.13	2.63	0.08	36.9
12-4	13.2	125	2214	6.80	152	0.364	0.66	0.95	0.084	1.47	73.5	-47.09	0.09	5.29	0.05	36.9
12-5	13.2	126	2429	6.74	127	0.369	0.61	1.04	0.076	1.67	21.0	-30.29	0.61	1.52	0.39	40.5
12-5	13.2	126	2429	6.74	127	0.369	0.61	1.04	0.076	1.67	41.0	-34.00	0.40	2.98	0.25	40.5
12-5	13.2	126	2429	6.74	127	0.369	0.61	1.04	0.076	1.67	52.0	-43.33	0.14	3.78	0.09	40.5

Table A-2 [continued]. All pressure fluctuation data.

Run	Gate (deg)	H (ft)	N (rpm)	Q (cfs)	T (ft-lb)	σ	Eff	ϕ_2	HP ₁₁	TRANSDUCER LOCATION - T1						
										Swirl Param	f (Hz)	RMS amp. (dBV)	(psi)	Freq. Param	Press Param	Shaft Freq.
13-1	10.2	120	1629	5.87	161	0.407	0.62	0.72	0.070	1.91	8.0	-38.78	0.23	0.67	0.19	27.2
13-1	10.2	120	1629	5.87	161	0.407	0.62	0.72	0.070	1.91	16.0	-44.05	0.13	1.33	0.10	27.2
13-1	10.2	120	1629	5.87	161	0.407	0.62	0.72	0.070	1.91	27.5	-49.03	0.07	2.29	0.06	27.2
13-2	10.2	122	1796	5.90	147	0.383	0.62	0.78	0.068	2.09	7.5	-30.55	0.59	0.62	0.49	29.9
13-2	10.2	122	1796	5.90	147	0.383	0.62	0.78	0.068	2.09	15.0	-42.54	0.15	1.24	0.12	29.9
13-2	10.2	122	1796	5.90	147	0.383	0.62	0.78	0.068	2.09	22.0	-49.51	0.07	1.82	0.06	29.9
13-2	10.2	122	1796	5.90	147	0.383	0.62	0.78	0.068	2.09	30.5	-51.38	0.05	2.53	0.04	29.9
13-2	10.2	122	1796	5.90	147	0.383	0.62	0.78	0.068	2.09	37.5	-47.51	0.08	3.11	0.07	29.9
13-3	10.2	123	1924	5.81	134	0.377	0.61	0.84	0.066	2.20	8.5	-28.64	0.74	0.72	0.63	32.1
13-3	10.2	123	1924	5.81	134	0.377	0.61	0.84	0.066	2.20	17.0	-42.47	0.15	1.43	0.13	32.1
13-3	10.2	123	1924	5.81	134	0.377	0.61	0.84	0.066	2.20	24.5	-41.97	0.16	2.06	0.14	32.1
13-3	10.2	123	1924	5.81	134	0.377	0.61	0.84	0.066	2.20	51.0	-45.61	0.10	4.30	0.09	32.1
13-4	10.2	124	2023	5.79	127	0.373	0.60	0.88	0.065	2.27	8.0	-30.65	0.59	0.68	0.50	33.7
13-4	10.2	124	2023	5.79	127	0.373	0.60	0.88	0.065	2.27	13.5	-38.31	0.24	1.14	0.21	33.7
13-4	10.2	124	2023	5.79	127	0.373	0.60	0.88	0.065	2.27	16.0	-39.75	0.21	1.35	0.18	33.7
13-4	10.2	124	2023	5.79	127	0.373	0.60	0.88	0.065	2.27	24.0	-40.21	0.20	2.03	0.17	33.7
13-4	10.2	124	2023	5.79	127	0.373	0.60	0.88	0.065	2.27	51.5	-41.21	0.17	4.35	0.15	33.7
13-5	10.2	124	2064	5.80	123	0.372	0.59	0.89	0.064	2.32	8.0	-30.03	0.63	0.67	0.54	34.4
13-5	10.2	124	2064	5.80	123	0.372	0.59	0.89	0.064	2.32	20.0	-31.42	0.54	1.69	0.46	34.4
13-6	10.2	124	2160	5.77	114	0.371	0.58	0.93	0.062	2.42	19.5	-31.12	0.56	1.65	0.48	36.0
13-6	10.2	124	2160	5.77	114	0.371	0.58	0.93	0.062	2.42	11.5	-37.22	0.28	0.98	0.24	36.0
13-6	10.2	124	2160	5.77	114	0.371	0.58	0.93	0.062	2.42	39.5	-41.78	0.16	3.35	0.14	36.0
13-6	10.2	124	2160	5.77	114	0.371	0.58	0.93	0.062	2.42	52.5	-42.75	0.15	4.45	0.13	36.0
13-6	10.2	124	2160	5.77	114	0.371	0.58	0.93	0.062	2.42	60.5	-44.06	0.13	5.13	0.11	36.0
13-7	10.2	127	2265	5.70	102	0.361	0.54	0.97	0.057	2.53	20.0	-34.65	0.37	1.72	0.33	37.8
13-7	10.2	127	2265	5.70	102	0.361	0.54	0.97	0.057	2.53	9.5	-37.68	0.26	0.82	0.23	37.8
14-1	12.2	120	1705	6.56	192	0.399	0.70	0.75	0.087	1.27	7.5	-34.94	0.36	0.56	0.24	28.4
14-1	12.2	120	1705	6.56	192	0.399	0.70	0.75	0.087	1.27	15.0	-46.57	0.09	1.12	0.06	28.4
14-2	12.2	120	1831	6.53	176	0.397	0.69	0.80	0.085	1.41	7.5	-28.75	0.73	0.56	0.49	30.5
14-2	12.2	120	1831	6.53	176	0.397	0.69	0.80	0.085	1.41	15.0	-43.06	0.14	1.12	0.09	30.5
14-2	12.2	120	1831	6.53	176	0.397	0.69	0.80	0.085	1.41	23.5	-50.36	0.06	1.76	0.04	30.5
14-2	12.2	120	1831	6.53	176	0.397	0.69	0.80	0.085	1.41	30.5	-45.17	0.11	2.29	0.07	30.5
14-2	12.2	120	1831	6.53	176	0.397	0.69	0.80	0.085	1.41	37.5	-49.43	0.07	2.81	0.05	30.5
14-2	12.2	120	1831	6.53	176	0.397	0.69	0.80	0.085	1.41	43.0	-48.64	0.07	3.22	0.05	30.5
14-2	12.2	120	1831	6.53	176	0.397	0.69	0.80	0.085	1.41	51.0	-45.55	0.11	3.82	0.07	30.5
14-3	12.2	122	2017	6.47	163	0.387	0.70	0.88	0.085	1.50	8.0	-28.29	0.77	0.61	0.53	33.6
14-3	12.2	122	2017	6.47	163	0.387	0.70	0.88	0.085	1.50	16.0	-41.52	0.17	1.21	0.11	33.6
14-3	12.2	122	2017	6.47	163	0.387	0.70	0.88	0.085	1.50	23.5	-46.56	0.09	1.78	0.06	33.6
14-4	12.2	124	2227	6.41	137	0.377	0.64	0.96	0.077	1.73	20.0	-31.48	0.53	1.53	0.37	37.1
14-4	12.2	124	2227	6.41	137	0.377	0.64	0.96	0.077	1.73	8.5	-35.45	0.34	0.65	0.24	37.1
15-1	14.2	117	1784	7.23	212	0.399	0.75	0.79	0.104	0.93	7.5	-31.27	0.55	0.51	0.30	29.7
15-1	14.2	117	1784	7.23	212	0.399	0.75	0.79	0.104	0.93	15.0	-43.72	0.13	1.02	0.07	29.7
15-2	14.2	119	2017	7.12	196	0.388	0.78	0.89	0.106	1.01	7.5	-29.04	0.71	0.52	0.40	33.6
15-2	14.2	119	2017	7.12	196	0.388	0.78	0.89	0.106	1.01	15.0	-46.23	0.10	1.03	0.06	33.6
15-2	14.2	119	2017	7.12	196	0.388	0.78	0.89	0.106	1.01	23.0	-49.45	0.07	1.58	0.04	33.6
15-2	14.2	119	2017	7.12	196	0.388	0.78	0.89	0.106	1.01	33.5	-50.30	0.06	2.30	0.03	33.6
15-2	14.2	119	2017	7.12	196	0.388	0.78	0.89	0.106	1.01	52.5	-55.37	0.03	3.61	0.02	33.6
15-2	14.2	119	2017	7.12	196	0.388	0.78	0.89	0.106	1.01	67.5	-56.14	0.03	4.64	0.02	33.6
15-3	14.2	123	2355	7.01	148	0.368	0.68	1.02	0.089	1.35	21.5	-31.34	0.54	1.50	0.32	39.3
15-3	14.2	123	2355	7.01	148	0.368	0.68	1.02	0.089	1.35	8.5	-36.59	0.30	0.59	0.17	39.3
15-3	14.2	123	2355	7.01	148	0.368	0.68	1.02	0.089	1.35	42.5	-39.56	0.21	2.97	0.12	39.3
16-1	15.2	120	2491	7.14	130	0.386	0.64	1.10	0.086	1.34	21.5	-31.95	0.51	1.47	0.28	41.5
16-1	15.2	120	2491	7.14	130	0.386	0.64	1.10	0.086	1.34	10.0	-35.39	0.34	0.69	0.19	41.5
16-1	15.2	120	2491	7.14	130	0.386	0.64	1.10	0.086	1.34	13.5	-34.94	0.36	0.93	0.20	41.5
16-1	15.2	120	2491	7.14	130	0.386	0.64	1.10	0.086	1.34	42.0	-37.81	0.26	2.88	0.14	41.5
16-2	15.2	122	2697	7.02	99	0.373	0.52	1.18	0.069	1.56	45.0	-29.81	0.65	3.14	0.38	45.0
17-1	16.2	113	1785	7.73	233	0.448	0.80	0.81	0.121	0.62	7.0	-31.95	0.51	0.44	0.24	29.8
17-1	16.2	113	1785	7.73	233	0.448	0.80	0.81	0.121	0.62	14.5	-44.08	0.13	0.92	0.06	29.8
17-1	16.2	113	1785	7.73	233	0.448	0.80	0.81	0.121	0.62	22.0	-53.36	0.04	1.39	0.02	29.8
17-1	16.2	113	1785	7.73	233	0.448	0.80	0.81	0.121	0.62	29.5	-52.31	0.05	1.87	0.02	29.8
17-2	16.2	115	2019	7.65	211	0.435	0.81	0.91	0.120	0.74	7.5	-28.23	0.78	0.48	0.38	33.7
17-2	16.2	115	2019	7.65	211	0.435	0.81	0.91	0.120	0.74	15.0	-44.54	0.12	0.96	0.06	33.7
17-2	16.2	115	2019	7.65	211	0.435	0.81	0.91	0.120	0.74	22.5	-51.70	0.05	1.44	0.03	33.7
17-2	16.2	115	2019	7.65	211	0.435	0.81	0.91	0.120	0.74	30.0	-56.66	0.03	1.92	0.01	33.7
17-2	16.2	115	2019	7.65	211	0.435	0.81	0.91	0.120	0.74	33.5	-50.85	0.06	2.14	0.03	33.7
17-3	16.2	119	2255	7.55	178	0.413	0.75	1.00	0.108	0.94	8.0	-30.11	0.63	0.52	0.31	37.6
17-3	16.2	119	2255	7.55	178	0.413	0.75	1.00	0.108	0.94	16.0	-39.46	0.21	1.04	0.11	37.6
17-3	16.2	119	2255	7.55	178	0.413	0.75	1.00	0.108	0.94	24.5	-40.82	0.18	1.59	0.09	37.6
17-3	16.2	119	2255	7.55	178	0.413	0.75	1.00	0.108	0.94	37.5	-43.71	0.13	2.43	0.07	37.6

APPENDIX B

MODEL-PROTOTYPE SAMPLE CALCULATION

SAMPLE CALCULATION

The results of Run 6-6 are used to illustrate the use of the dimensionless parameters for calculation of prototype pressure fluctuations from model test results. The data for this run are:

$$\begin{aligned}
 GO &= 20.2^\circ \\
 H &= 116.8 \text{ ft} \\
 N &= 2440 \text{ rpm} \quad (\omega = 127.8 \text{ rad/sec}) \\
 Q &= 8.99 \text{ cfs} \\
 T &= 201 \text{ ft-lb} \\
 BHP &= 93 \text{ hp} \quad (P = 51150 \text{ ft-lb/sec}) \\
 D_2 &= 0.738 \text{ ft} \\
 D_3 &= 0.788 \text{ ft}
 \end{aligned}$$

The value of the draft tube swirl parameter is calculated from these data using Eq. (3-8) and (3-12):

$$\left(\frac{\Omega_2 D_3}{\rho Q^2} \right)_m = \frac{\Omega_1 D_3}{\rho Q^2} - \frac{P D_3}{\omega \rho Q^2} \quad (3-8)$$

$$\left(\frac{\Omega_2 D_3}{\rho Q^2} \right)_m = 59(GO)^{-1.18} - \frac{P D_3}{\omega \rho Q^2}$$

$$\left(\frac{\Omega_2 D_3}{\rho Q^2} \right)_m = 59(20.2)^{-1.18} - \frac{(51150 \text{ ft-lb/sec})(0.788 \text{ ft})}{(127.8 \text{ rad/s})(1.94 \text{ slug/ft}^3)(8.99 \text{ cfs})^2}$$

$$\left(\frac{\Omega_2 D_3}{\rho Q^2} \right)_m = 0.69$$

The dominant pressure fluctuation at this test point was at a frequency of 9.0 Hz with an amplitude of 1.17 psi (rms). The resulting frequency and pressure parameters are:

$$\left(\frac{f D_3^3}{Q} \right)_m = \frac{(9.0 \text{ Hz})(0.788 \text{ ft})^3}{8.99 \text{ cfs}} = 0.49$$

$$\left(\frac{D_3^4 \sqrt{(p')^2}}{\rho Q^2} \right)_m = \frac{(0.788 \text{ ft})^4 (1.17 \text{ psi})(144 \text{ psf/psi})}{(1.94 \text{ slug/ft}^3)(8.99 \text{ cfs})^2} = 0.41$$

The synchronous speed and runner dimensions for the prototype unit are:

$$N = 85.7 \text{ rpm } (\omega = 8.97 \text{ rad/sec})$$

$$D_2 = 31.78 \text{ ft}$$

$$D_3 = 29.77 \text{ ft}$$

The operating point of the prototype unit corresponding to Run 6-6 is calculated by setting the speed ratio, unit power, and unit discharge for the model and prototype equal to one another, and then solving for the prototype head, output power, and discharge.

$$(\phi_2)_m = (\phi_2)_p$$

$$\left(\frac{\pi N D_2}{60 \sqrt{2gH}} \right)_m = \left(\frac{\pi N D_2}{60 \sqrt{2gH}} \right)_p$$

$$\frac{\pi(2440 \text{ rpm})(0.738 \text{ ft})}{60 \sqrt{2(32.2 \text{ ft/sec}^2)(116.8 \text{ ft})}} = \frac{\pi(85.7 \text{ rpm})(29.77 \text{ ft})}{60 \sqrt{2(32.2 \text{ ft/s}^2)H_p}}$$

$$H_p = 235 \text{ ft}$$

$$(HP_{11})_m = (HP_{11})_p$$

$$\left(\frac{BHP}{D_2^2 H^{3/2}} \right)_m = \left(\frac{BHP}{D_2^2 H^{3/2}} \right)_p$$

$$\frac{93 \text{ hp}}{(0.738 \text{ ft})^2 (116.8 \text{ ft})^{3/2}} = \frac{BHP_p}{(29.77 \text{ ft})^2 (235 \text{ ft})^{3/2}}$$

$$BHP_p = 432000 \text{ hp}$$

$$P_p = 238 \times 10^6 \text{ ft-lb/sec}$$

$$(Q_{11})_m = (Q_{11})_p$$

$$\left(\frac{Q}{D_2^2 H^{1/2}} \right)_m = \left(\frac{Q}{D_2^2 H^{1/2}} \right)_p$$

$$\frac{(8.99 \text{ cfs})}{(0.738 \text{ ft})^2 (116.8 \text{ ft})^{1/2}} = \frac{Q_p}{(29.77 \text{ ft})^2 (235 \text{ ft})^{1/2}}$$

$$Q_p = 20700 \text{ cfs}$$

Recalculation of the draft tube swirl parameter at this operating point shows that the prototype swirl is equal to the model swirl, as expected.

$$\left(\frac{\Omega_2 D_3}{\rho Q^2}\right)_p = 59(GO)^{-1.18} - \frac{P D_3}{\omega \rho Q^2}$$

$$\left(\frac{\Omega_2 D_3}{\rho Q^2}\right)_p = 59(20.2)^{-1.18} - \frac{(238 \times 10^6 \text{ ft-lb/sec})(31.78 \text{ ft})}{(8.97 \text{ rad/s})(1.94 \text{ slug/ft}^3)(20700 \text{ cfs})^2}$$

$$\left(\frac{\Omega_2 D_3}{\rho Q^2}\right)_p = 0.69$$

Equations (3-21) and (3-22) are then used to compute the amplitude and frequency of the pressure fluctuation in the prototype unit:

$$\left(\sqrt{(P')^2}\right)_p = \left(\frac{D_3^4 \sqrt{(P')^2}}{\rho Q^2}\right)_m \left(\frac{\rho Q^2}{D_3^4}\right)_p \quad (3-21)$$

$$\left(\sqrt{(P')^2}\right)_p = (0.41) \frac{(1.94 \text{ slug/ft}^3)(20700 \text{ cfs})^2}{(31.78 \text{ ft})^4}$$

$$\left(\sqrt{(P')^2}\right)_p = 334 \text{ lb/ft}^2$$

$$\left(\sqrt{(P')^2}\right)_p = 2.32 \text{ psi}$$

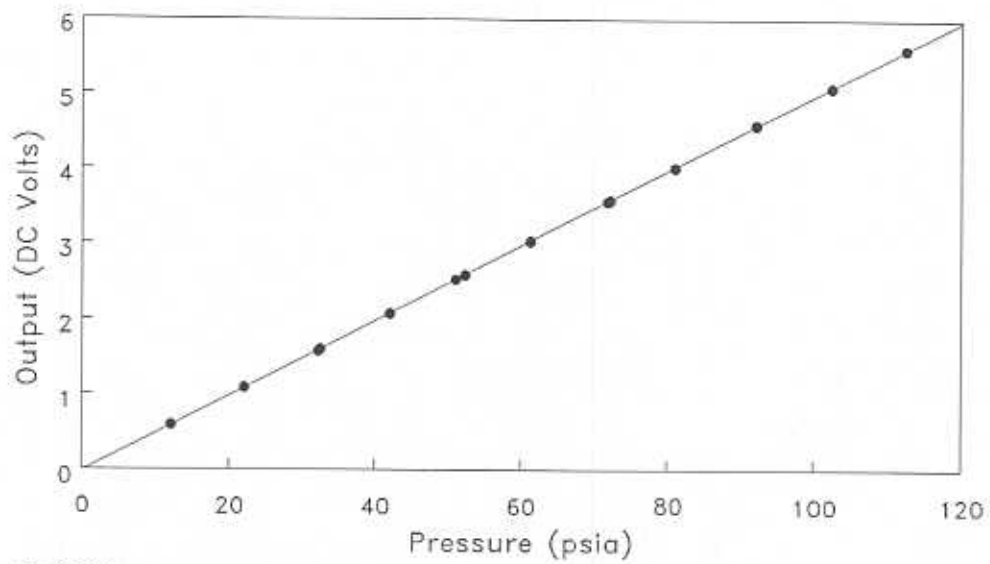
$$f_p = \left(\frac{f D_3^3}{Q}\right)_m \left(\frac{Q}{D_3^3}\right)_p \quad (3-22)$$

$$f_p = (0.49) \left(\frac{20700 \text{ cfs}}{(31.78 \text{ ft})^3}\right)$$

$$f_p = 0.32 \text{ Hz}$$

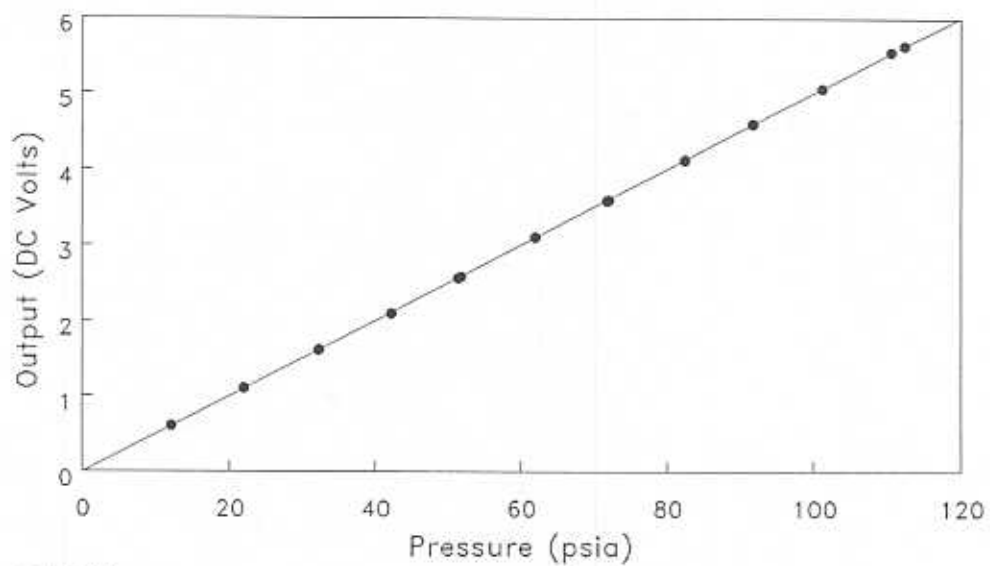
APPENDIX C
CALIBRATIONS

Transducer Location T1
Endevco #B58H



10/20/89
Signal Conditioner AC44

Transducer Location T2
Endevco #B75H



10/20/89
Signal Conditioner AC43

Figure C-1. Pressure transducer calibrations.

Table C-1. Wicket gate calibration.

Gate Opening (degrees)	Counter Reading
6.2	99912
7.2	99895
8.2	99877
9.2	99860
10.2	99844
11.2	99826
12.2	99810
13.2	99794
14.2	99776
15.2	99760
16.2	99744
17.2	99725
18.2	99708
19.2	99690
20.2	99673
21.2	99655
22.2	99636
23.2	99619
24.2	99601
25.2	99583
26.2	99564
27.2	99547
28.2	99528
29.2	99511
30.2	99494
31.2	99477
32.2	99460
33.2	99444
34.2	99428
35.2	99413
36.2	99399